

See discussions, stats, and author profiles for this publication at: <https://www.researchgate.net/publication/312577690>

In Situ Anchor Ice, Frazil and River Ice Cover Development: Perspectives from Acoustic Profile Studies

Technical Report · January 2017

DOI: 10.13140/RG.2.2.35624.78083

CITATION

1

READS

52

1 author:



J.R. Marko

ASL Environmental Sciences

80 PUBLICATIONS 565 CITATIONS

SEE PROFILE



Technical Report

In Situ Anchor Ice, Frazil and River Ice Cover Development: Perspectives from Acoustic Profile Studies

J.R. Marko¹, M. Jasek² and D.R. Topham¹

¹*ASL Environmental Sciences Inc., Saanichton, BC, Canada*

²*BC Hydro, Burnaby, BC, Canada*

ASL File: RD-IPS-16 (4)

January 16, 2017

ASL Environmental Sciences Inc.

1-6703 Rajpur Pl., Saanichton, BC, Canada V8M 1Z5, Tel: 1 (250) 656-0177

Web: www.aslenv.com

¹Corresponding Author email: jmarko@aslenv.com

Preface

This Report was intended to complete a trilogy of publications on applications of acoustic technology to the study of ice formation in larger rivers. The first part (Marko and Topham, 2015) verified the utilized basic acoustic measurement technique through laboratory experiments on suspensions of precision-cut plastic discs. The second part (Marko et al., 2015) reported actual acoustic data obtained on frazil ice formation and content in the Peace River. The Technical Report presented here represents the third part of the trilogy, which interprets a broader body of Peace River acoustic and other data in terms of physical processes active during the initial stages of freeze-up.

An earlier version of this Report was submitted to Cold Regions Science and Technology in April, 2015. Three additional versions of the document were subsequently successively submitted to CRST implementing reviewer-requested revisions and additions. These changes significantly improved the manuscript and allowed introduction of new information which greatly clarified interpretation of the included results. Nevertheless, in early January, 2017, the manuscript was finally rejected by a majority vote of a closely split panel of five reviewers. The justification for this decision was that, although the work was of some interest, the utilized acoustic techniques were not validated in the field and the offered interpretations were overly speculative.

The authors have full confidence in the utilized acoustic measurements since the applied techniques have been well established in other, closely-related, fields. Additionally, the demonstrated consistency of a broad range of acoustic and non-acoustic data with the offered interpretations provides strong arguments for the suggested revisions in the relationships assumed to link frazil-, anchor- and river surface-ice. Consequently, we believe the current manuscript is worthy of wide distribution as a replacement and extension of a December, 2015 ASL Technical Report previously posted on the ResearchGate site.

Marko, J. R. Topham, D.R., 2015. Laboratory measurements of acoustic backscattering from polystyrene pseudo-ice particles as a basis for quantitative frazil characterization. *Cold Reg. Sci. Technol.* 112, 66-86.

Marko, J.R., Jasek, M., Topham, D.T, 2015. Multifrequency Analyses of 2011-2012 Peace River SWIPS frazil backscattering data. *Cold Reg. Sci. Technol.* 110, 102-119.

Abstract

A recent SWIPS (Shallow Water Ice Profiling Sonar) acoustic backscattering study of 2011-2012 ice conditions in the Peace River (Marko et al., 2015) identified major differences between measured and modelled frazil fractional volumes. The shortfall in the observed fractional volumes was suggested to be evidence of massive anchor ice formation deliberately excluded from model simulations. This assertion is further developed with detailed comparisons of simulated and measured SWIPS and river parameters. Wide variations were apparent in model overestimation of fractional volume as functions of time, with this parameter varying on temporal scales largely absent from the simulated results. Calculations of thermodynamic balance at frazil initiation, combined with requirements of self-consistency, dictated that this variability be accompanied by abundant *in situ* riverbed anchor ice growth. Independent verification of this interpretation and growth estimates were obtained from studies of water levels and acoustic beam blockages produced by anchor ice on SWIPS transducers. A simple “overflow” model of anchor ice layer development related this ice to anchor ice thickness on the adjacent riverbed, linking its growth to atmospheric heat losses during supercooling periods. A threshold for blockage onset was established in terms of riverbed ice thickness. Applications of this threshold to SWIPS frazil data from intervals not associated with blockages suggested that cooling rates were major determinants of attainable thicknesses of stable anchor ice. It was concluded that *in situ* anchor ice growth is the principal direct source of Peace River seasonal ice cover development. The implications of these results for river ice research and management are discussed.

1. Introduction

Anchor ice presence in freezing rivers has been established by direct observations (Arden and Wigle, 1972; Hirayama et al., 1997; Liu et al., 2004; Kempema, 2008) as well as from the impacts of such ice on hydroelectric power production (Marcotte and Robert, 1986) and deployed instrumentation (Jasek et al., 2005; Marko and Jasek, 2010a). Rare quantitative measures of this presence include reports of 0.3 m to 0.5 m layers on a submerged wire screen (Arden and Wigle, 1972) and 2 to 3 m anchor ice dams in a shallow river (Liu et al., 2004). Ice slabs as thick as 80 cm were observed (Parkinson, 1984) rising off the St Lawrence River riverbed. Nevertheless, the absence of quantitative field data linking anchor ice to frazil and other ice forms in medium- and larger-sized rivers has inhibited its confident inclusion in river ice models. This situation is partly due to the lack, until recently (Marko and Topham, 2015; Marko et al., 2015a), of a reliable methodology for obtaining detailed sub-surface ice data, particularly in rivers deep enough to support heavy ice cover growth. This problem is addressed in the present work by detailed analyses of 2011-2012 Peace River SWIPS (Shallow Water Ice Profiling Sonar) data.

Recent considerations of such data focused on evidence (Marko et al., 2015a) that estimated peak values of frazil fractional volume were, roughly, 40 times smaller than values simulated with a BC Hydro Operational CRISSP1D ice growth model (Shen, 2005; Jasek et al., 2011). The latter model was tuned to approximately reproduce volumes and upstream advance rates of surface ice as estimated from several years of Peace River observational data. Obtaining satisfactory agreement required disabling the CRISSP1D anchor ice simulation module and attributing consequent ice cover growth solely to surface accumulations of rising frazil (Jasek et al., 2011). The low concentrations of frazil detected in the SWIPS measurements raised possibilities for an alternative interpretation in which anchor ice plays a dominant role in ice cover development. This role would require intense anchor ice growth during all supercooling intervals followed by subsequent buoyancy- and sub-strata erosion-driven upward movement (Liu et al., 2008) toward the river surface. Physical connections between anchor ice and surface ice cover development are explored through detailed analyses of the Marko et al. (2015a) results which, in addition to frazil fractional volumes and atmospheric parameters, included previously unreported water-temperature and -level data and quantitative evidence of anchor ice impacts on SWIPS measurements. The objective of these efforts will be to clarify and quantify interlinkages among the ice constituents of current river ice models.

2. Methodology

Ice profiling measurements were carried out, as described by Marko et al. (2015a), using backscattered returns from sound pulses emitted at four different acoustic frequencies (Table 1) by an upward-looking ASL Environmental Sciences SWIPS instrument.

Table 1. Basic acoustic details of the four utilized SWIPS channels

Channel	Acoustic Frequency (kHz)	-3 dB Beamwidth (°)
1	125	8
2	235	6
3	455	7
4	774	7

The transducers for three of the channels (1, 3 and 4) were mounted in a common head while the channel 2 transducer was displaced horizontally and positioned separately about 18 cm from the

other transducers. All instrument components were mounted inside a truncated pyramid enclosure (Fig.1) constructed within an exterior shell of ice attachment-resistant Teflon. This structure was thermally insulated on its interior walls and bolted to four 6 mm thick steel plates. A 500 watt heater elevated interior water temperatures to discourage the anchor ice attachments which have previously ([Marko and Jasek, 2010a](#)) physically destabilized instruments and blocked profiling. Further design details and descriptions of the deployment location are given by [Marko and Jasek \(2010b\)](#).

SWIPS profile data as well as water velocity profiles, water levels and water temperatures (acquired with a co-deployed (Fig. 1) Teledyne RDI Sentinel ADCP instrument) were transmitted to a shore station through an armoured 50m power and data/control cable. Although the temperature sensor had a nominal resolution of 0.01 °C, necessary reliance on the manufacturer's calibration and proximity to heated water inside the enclosure, limited use to broader but critically useful tracking of river cooling and warming trends. Some assurance that impacts of applied heating were minimal can be drawn from the fact that, in all Intervals, ADCP temperatures following frazil onset remained at the freezing point to within the +/- 0.01 °C sensor resolution. In particular, the time rate of change of temperature prior to frazil onset can safely be assumed to be insensitive to external heating effects, yielding accuracies sufficient for the present work.

The instrument package was deployed in 5 m water depths approximately 25 m off the south bank of the Peace River. SWIPS operations cycled through all four frequencies: successively emitting 100-150 microsecond duration pulses at 1 Hz and recording range-sampled signal voltages from backscattered acoustic returns. Internal averaging was applied to successive pairs of range samples, producing 16-bit digitized signal voltages representative of 4 cm-deep water column cells. These voltages were converted into measures of either target strength (TS) in dB re 1 µPa or volume backscattering coefficients, Sv, in m⁻¹ for distributed targets.

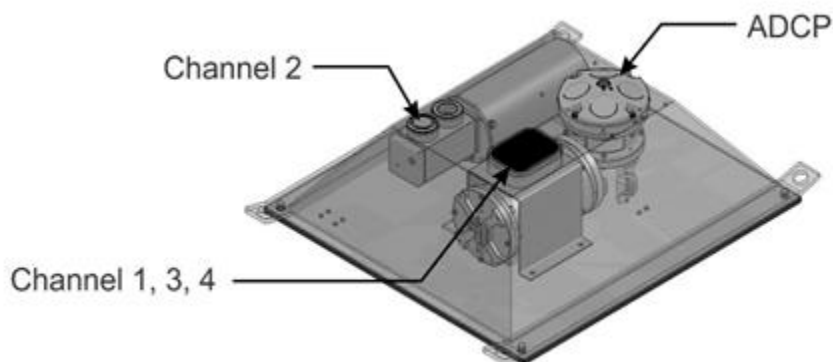


Fig. 1. The deployed instrument package showing the locations of the multifrequency SWIPS and ADCP current profiler including the locations of the SWIPS transducers for channels 1-4.

Vertical profiles of frazil fractional volume, F, were derived using ASL's RUNSWIPS algorithm ([Marko et al. 2015a](#)) on Sv data acquired in channels 1, 3 and 4. The accuracies of these estimates were discussed by [Marko et al. \(2015\)](#) both in relation to the original laboratory calibrations of [Marko and Topham \(2015\)](#) and with respect to the implications of the extremely low residuals attained between optimal RUNSWIPS fits to multifrequency data and expectations from a universally used scattering theory. The laboratory work closely paralleled methods widely used in field-verified sediment -and zooplankton-profiling studies and was fully compatible with the multifrequency residual results which suggested fractional volume estimation uncertainties were on the order of +/-25%. On the basis of the available river velocity data, the 10-minute-averaged values of F utilized in the analyses were representative of, roughly, 1 km long sampling areas upstream of the SWIPS site. Averaged values were computed for measurements at levels approximately 1.3, 2.6, 3.6 and 4.25 to 4.55 m above the

riverbed in water depths ranging between 4.7 and 5.0 m. F values at these and other tested water column levels were highly correlated and, except for regions very close to the river surface (often contaminated by returns from surface ice), rarely deviated from each other by more than 20%. Fractional volumes tended to increase gradually with height in the water column. These characteristics allowed use of mid-water (2.3m above the transducers) SWIPS estimates for comparisons with the water-column mean F values simulated by the CRISSP1D model (Shen, 2005). All simulations were performed in the BC Hydro operational mode (Jasek et al., 2011) without further adjustments, utilizing inputs of water temperature and discharge data, available at hourly intervals from a hydroelectric site approximately 370 km upstream of the SWIPS instrument. Hourly surface air temperature inputs were obtained (to set model boundary conditions) near river gauges 7 km and 100 km downstream of the SWIPS location as well as 94, 226, 278 and 362 km upstream. The model utilized a 30 minute time step and linear interpolation of hourly input data. Detailed discussions of simulation procedures were provided by Jasek et al. (2011). Analyses were confined to the five earliest of the seven frazil Intervals processed by Marko et al. (2015a). These Intervals (Table 2) all preceded ice cover consolidation and were representative of early winter frazil processes.

Table 2. Analyzed frazil intervals

Interval	Start and end times, dates	Duration (h)
1	17:14 Nov. 20 to 01:04 Nov 21	8
2	01:34 Jan.3 to 12:55 Jan.3	11
3	19:34 Jan 14 to 23:57 Jan 15	29
4	07:34 Jan.25 to 13:45 Jan.26	30
5	23:04 Feb 6 to 04:04 Feb. 7	5

3. Frazil and anchor ice: insights from comparisons of SWIPS and field data with model simulations

3.1 Comparisons and implications for river ice development processes

In principle, connections between suspended frazil and other river ice components can be evaluated by adjusting frazil-related ice model parameters to maximize the compatibility of the simulations with measurements on these components. Applications of this approach by Jasek et al. (2011) with the Peace River Operational CRISSP1D model utilized comparisons with the only readily available measured ice parameters: surface ice cover-volume and -edge position. The apparent agreement, attained without accounting for anchor ice growth, was taken as evidence that such growth was inconsequential and could be neglected without significant degradation of model performance. Discovery (Marko et al., 2015a) of major discrepancies between estimated and simulated peak frazil fractional volumes, F, undermined this conclusion, motivating closer examination of ice constituent inter-relationships.

The ADCP water temperature data provided an additional basis for assessing CRISSP1D simulations. These data are plotted in Fig. 2 for times prior to seasonal ice consolidation along with temperatures simulated for the deployment site and as measured at the upstream hydroelectric dam outlet. The plotted results confirm the model's capability for broadly reproducing water temperatures at the measurement site and for validating CRISSP1D representations of net energy exchanges between the river and its external environment. Likewise, Jasek et al.'s (2011) reproductions of observed surface ice parameter values implied adequate model treatment of total ice production. By default, these successes suggest that CRISSP1D frazil over-prediction may have arisen from deficiencies in the

treatment of energy and mass exchanges among different river ice components. The origins of such deficiencies are sought below in comparisons of measurement-derived- and simulated-frazil contents.

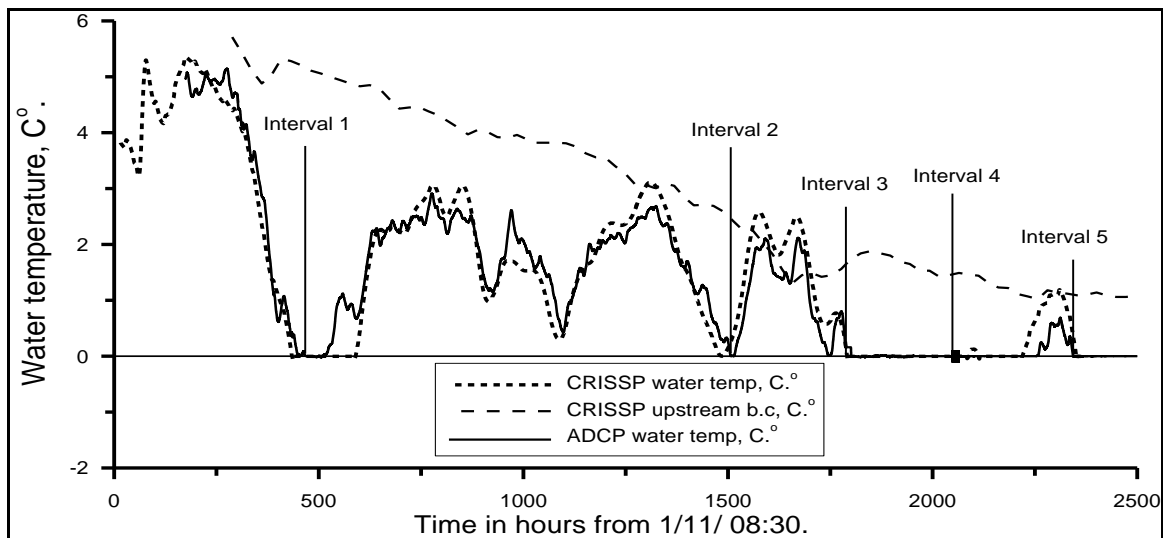


Fig. 2. Comparisons between the measured and simulated water temperatures at the SWIPS site plus water temperature data (upstream b.c.) measured at the upstream dam outlet. Vertical markers denote beginnings of frazil Intervals.

Although the model predicts the onset of surface ice formation on time scales suitable for operational forecasting (within one day or so), the attained precisions are insufficient to reliably match the timings of the observed frazil intervals. This limitation is a consequence of the large geographical extent of the modelled region and the sparse network of environmental inputs. Thus, although atmospheric data were acquired at sites along the extensive reach of river separating the dam outlet from the SWIPS site, local conditions between these sites may deviate considerably from interpolated model outputs due to unrepresented local variations in cloud cover, wind chill and snowfall. Additional variability can arise from heat exchanges between river bed sediments and the water column which were neglected in the simulations. The principal impacts of these higher order influences are to introduce errors in the timings of simulated initial crossings of the 0°C water isotherm.

These limitations of the operational model complicated direct comparisons of simulations with SWIPS-based estimates of frazil fractional volume. In particular, for timing differences in excess of 1 or 2 hours, simulations may have been driven by atmospheric and upstream boundary conditions which differed significantly from those attained in corresponding observed frazil events. As a consequence, simulation/observation differences in frazil content could include contributions from mismatches in, assumed and actual forcing conditions.

The sensitivity of simulated timing accuracy to differences between simulated and actual water temperatures is evident in the data plotted in Fig. 3.

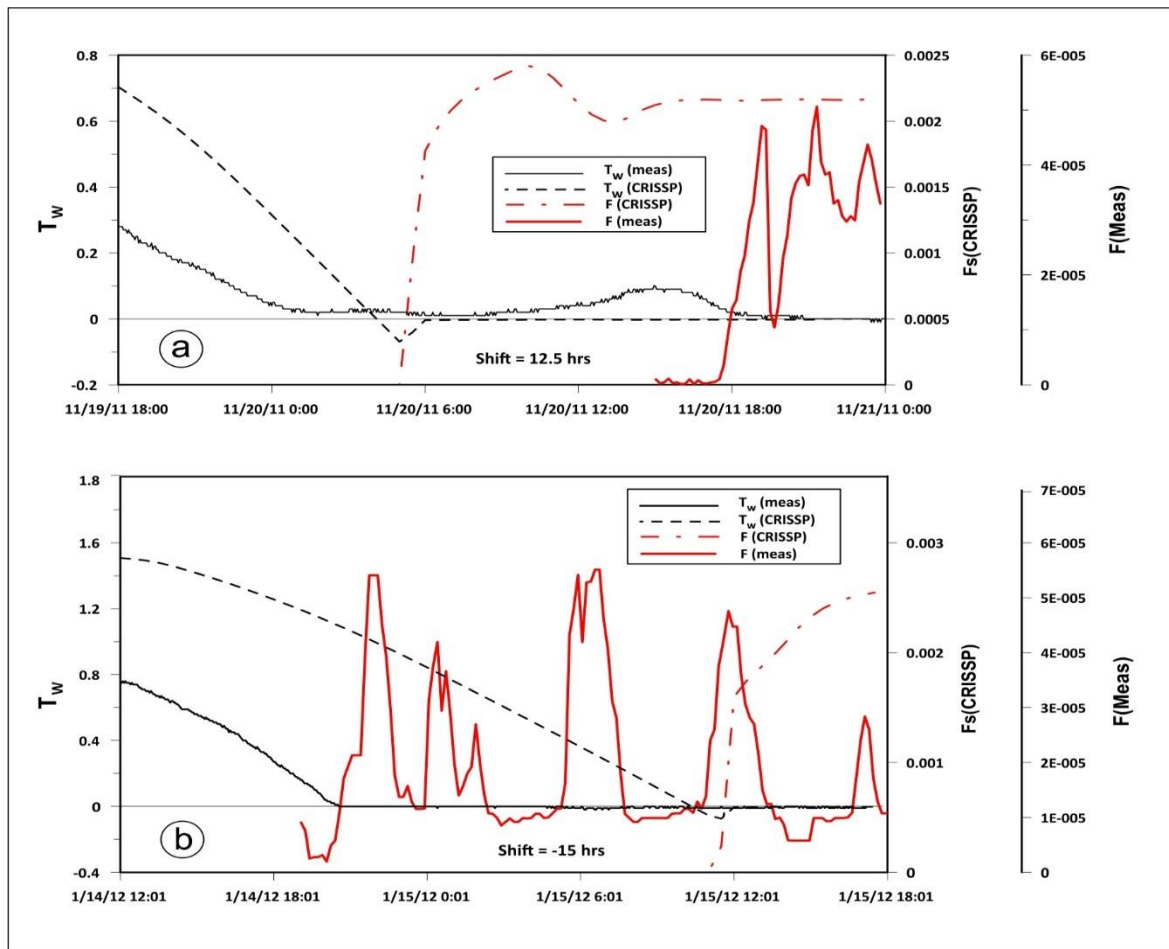


Fig 3. Plots of measurement-derived ($F(\text{meas})$ and $T_w(\text{meas})$) and simulated ($F(\text{CRISSP})$ and $T_w(\text{CRISSP})$) frazil fractional volume and water temperature quantities for a) frazil Interval 1 and b) frazil Interval 3. The simulated quantities correspond to model outputs prior to application of the shifts in time which were later used (in Figs. 4 and 7) to allow side by side comparisons between $F(\text{meas})$ and an equivalent “shifted” simulated quantity, $F_s(\text{CRISSP})$.

Curves are included depicting water temperature and frazil fractional volume results both as simulated by the CRISSP1D model and as derived from measurements ($T_w(\text{meas})$) with the ADCP temperature sensor and as extracted ($F(\text{meas})$) from SWIPS data. In Fig. 3a, corresponding to Interval 1 data associated with a prematurely simulated frazil onset, measured and simulated temperatures simultaneously approached zero (within sensor resolution). Nevertheless persisting slight elevations of $T_w(\text{meas})$ delayed actual onset by 12.5 hours. Interval 3 data in Fig 3b shows a temporal shift in the opposing direction arising from unanticipated early arrivals of cold water which caused the simulation results to lag observations by 15 hours.

Similar reviews of water temperature and frazil content results from our four most definitive frazil Intervals established the presence of time shifts, τ , of +12.65 h, -15 h, -10.75 h and +3.5 h, for Intervals 1, 3, 4 and 5, respectively, with positive (negative) offsets indicative of observations lagging (leading) corresponding simulations. The observed ($F(\text{meas})$) and shifted simulated ($F_s(\text{CRISSP})$) frazil volume concentrations are plotted in Figs. 4-7, using separate vertical axes to account for the previously noted (Marko et al., 2015a) nearly two orders of magnitude mismatch in simulated and estimated fractional volume magnitudes.

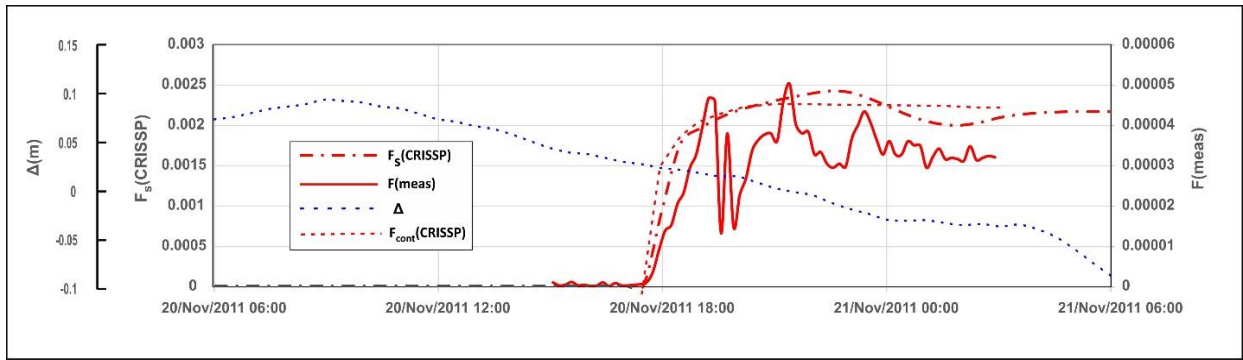


Fig.4. Comparisons of Interval 1 fractional volumes (Marko et al., 2015) as measured ($F(\text{meas})$) and simulated ($F_s(\text{CRISSP})$). The plot of $F_s(\text{CRISSP})$ was shifted back in time by 12 h to achieve approximate coincident positioning in time with $F(\text{meas})$. The two quantities are, respectively, representative of regions 2.3 m above the SWIPS instrument and water column mean values. Two additional curves include: $F_{\text{cont}}(\text{CRISSP})$ representing an artificially triggered simulated frazil Interval which is coincident with the observed Interval and driven by fully contemporary post-onset model input data; and Δ which depicts differences between 10-point running averaged local water levels and levels simulated by CRISSP1D neglecting anchor ice formation.

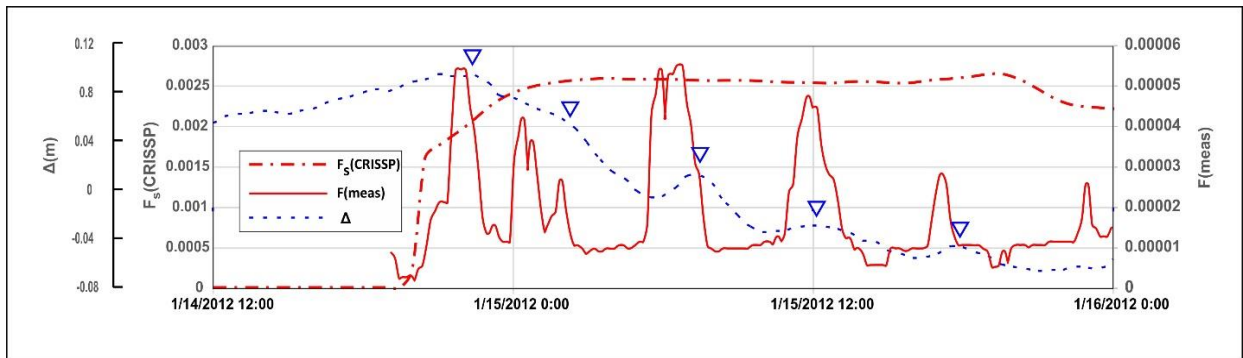


Fig.5. Comparisons of Interval 3 fractional volumes (Marko et al., 2015) as measured ($F(\text{meas})$) and simulated ($F_s(\text{CRISSP})$). The plot of $F_s(\text{CRISSP})$ was shifted ahead in time by 15 h to allow approximate coincident positioning in time with $F(\text{meas})$. The two quantities are, respectively, representative of regions 2.3 m above the SWIPS instrument and water column mean values. The additional, blue, curve represents Δ , the difference between 10-point running averaged local water levels and levels simulated in the absence of anchor ice formation by the CRISSPID model. Inverted triangles denote the central positions of the local anchor ice-generated water level peaks.

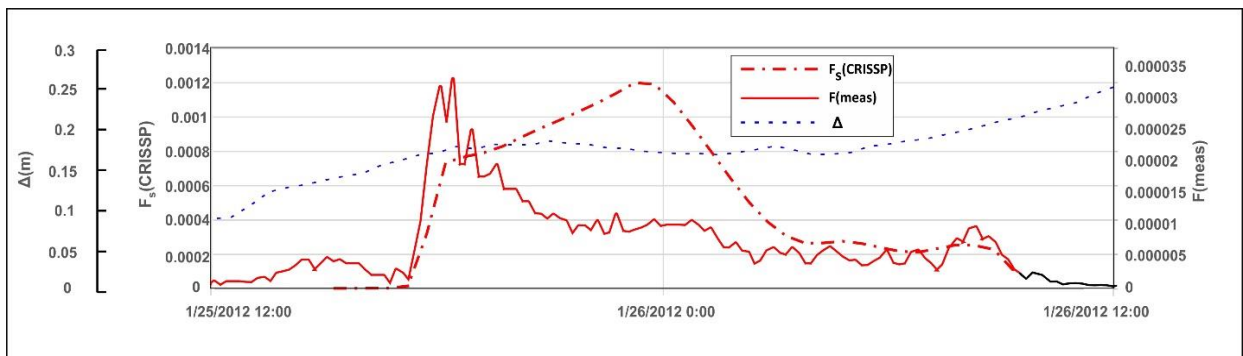


Fig.6. Comparisons of Interval 4 fractional volumes (Marko et al., 2015) as measured ($F(\text{meas})$) and simulated ($F_s(\text{CRISSP})$). The plot of $F_s(\text{CRISSP})$ was shifted ahead in time by 11 h to allow approximate coincident positioning in time with $F(\text{meas})$. The two quantities are, respectively, representative of regions 2.3 m above the SWIPS instrument and water column mean values. The additional curve represents Δ , the difference between 10-point running averaged local water levels and levels simulated in the absence of anchor ice formation by the CRISSPID model.

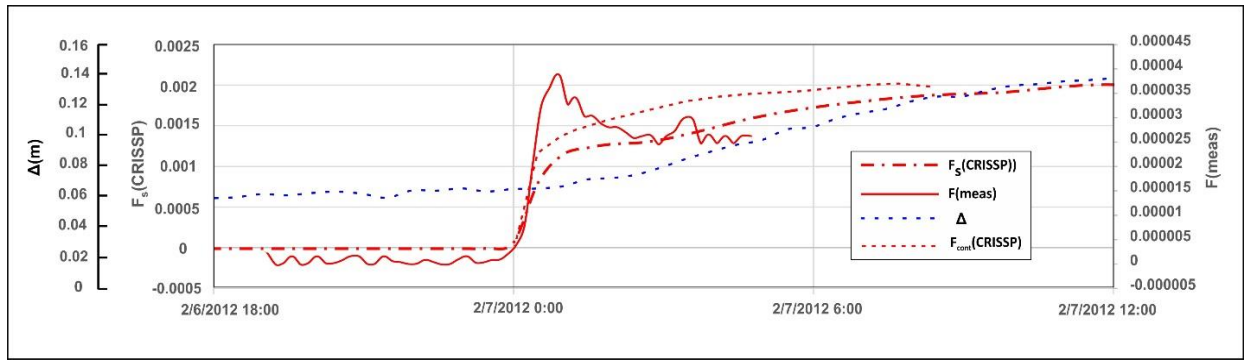


Fig.7. Comparisons of Interval 5 fractional volumes (Marko et al., 2015) as measured ($F(\text{meas})$) and simulated ($F_s(\text{CRISPP})$). The plot of $F_s(\text{CRISPP})$ was shifted back in time by 3.5 h to achieve approximate coincident positioning in time with $F(\text{meas})$. The two quantities are, respectively, representative of regions 2.3 m above the SWIPS instrument and water column mean values. Two additional curves include: $F_{\text{cont}}(\text{CRISPP})$ representing an artificially triggered simulated frazil Interval which is coincident with the observed Interval and driven by fully contemporary post-onset model input data; and Δ which depicts differences between 10-point running averaged local water levels and levels simulated by CRISPP 1D neglecting anchor ice formation.

Visual comparisons with measurement based fractional volumes were facilitated by forcing the sharp rises in the shifted simulated curves to coincide with the equivalent features in their observational counterparts. The listed shifts are significant and, as noted above, introduce differences in the atmospheric temperature (T_a) inputs which, alternatively, drive the shifted simulated- and observed- $F(t)$ relationships. The magnitudes of the temperature differences can be seen in the common plots (Fig.8a-d) of model air temperature inputs during corresponding observed and simulated frazil Intervals. In this Fig., inputs during actual frazil Intervals are denoted as $T_a(t)$ while the simulation inputs, underlying the $F_s(\text{CRISPP})$ plots of Figs. 4-7, are labelled as $(T_a(t + \tau))$ to denote inclusion of the shifts which facilitate visual comparisons with $F(\text{meas})$.

In assessing the impacts of $T_a(t)$ and $T_a(t + \tau)$ differences on simulation accuracy, it is to be noted that the critical CRISPP1D forcing element, the river surface heat flux, Φ , is expressed in terms of T_w and T_a as:

$$\Phi = K(T_w - T_a)(1 - C_i), \quad [1]$$

where C_i denotes the fractional surface ice coverage and K is an operationally determined coefficient. Consequently, during frazil Intervals (when T_w is effectively 0°C), fractional changes in Φ and T_a are nearly identical. Given this near-equality, the data in Fig. 8 suggest that, except for the anomalous Interval 4, differences in shifted simulated- and actual-forcings were, typically, on the order of 15%. Such estimates were further tested by additional simulations modified to reproduce the observed timings of corresponding frazil onsets using fully contemporary model inputs (i.e. represented by the $T_a(t)$ data in Fig. 8). This required appropriately timed artificial increases in the model's upstream dam water temperature inputs for Intervals 1 and 5 which were characterized by premature (relative to observations) frazil onsets. (Negative time shifts could not be easily accommodated by our simple modification device.) The applied increases were 15 h in duration and 2.1°C (Interval 1) and 0.25°C (interval 5) in magnitude. The resulting delays in simulated supercooling onsets assured that the environmental forcings during the modified frazil Interval simulations were identical to those present during acquisition of the corresponding $F(\text{meas})$ results. Frazil fractional volumes simulated for Interval 1 and 5, denoted by $F_{\text{cont}}(\text{CRISPP})$, are included in Figs 4 and 7 for comparisons with corresponding $F(\text{meas})$ and $F_s(\text{CRISPP})$ curves. The close similarities between corresponding $F_{\text{cont}}(\text{CRISPP})$ and $F_s(\text{CRISPP})$ curves support the above estimates of fractional errors introduced by model input timing errors. Clearly, such errors had little impact upon the characteristic magnitudes

and time dependences of simulated frazil contents: justifying judicious direct comparisons of measured and simulated river ice-parameters.

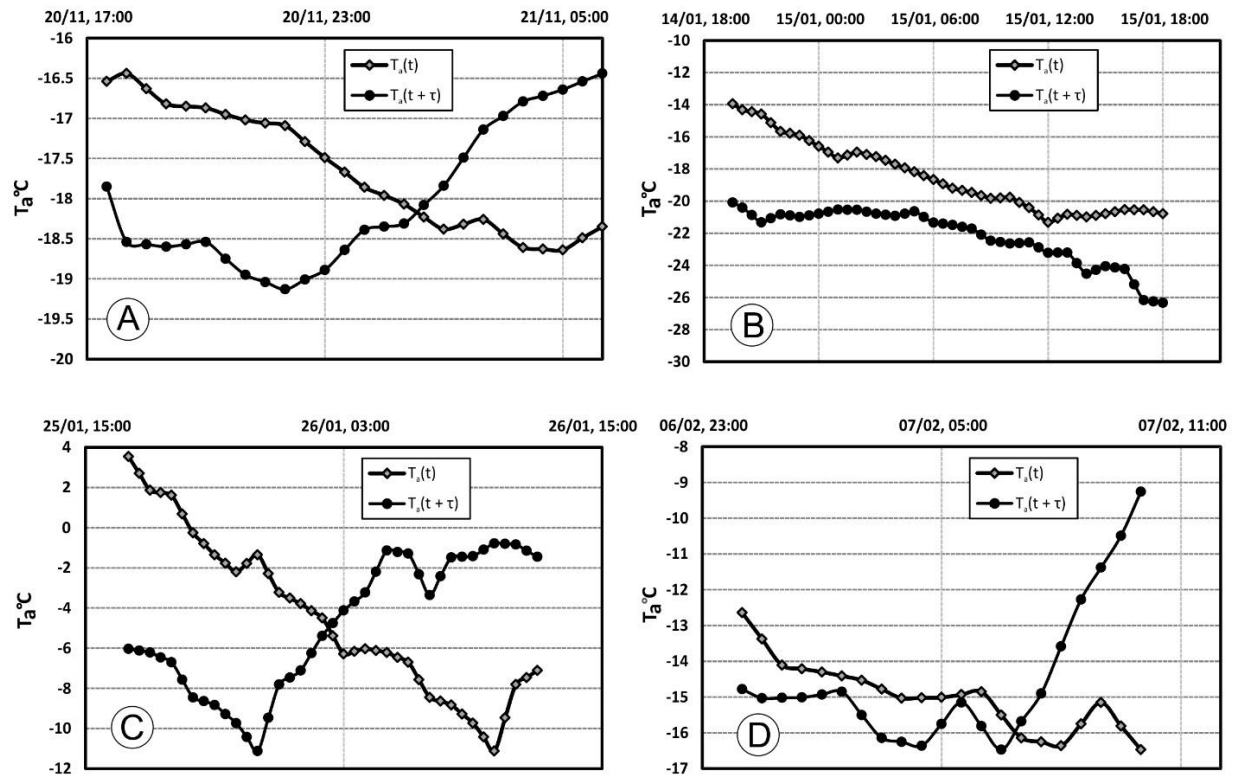


Fig. 8. Plots of CRISSP1D air temperature (T_a) inputs corresponding to times immediately preceding and during: a) frazil Interval 1; b) frazil Interval 3; c) frazil Interval 4 and d) frazil Interval 5. Additional temperature curves are included in each case (designated as $T_a(t + \tau)$) where $\tau = 12, -11, -15$ and 3.5 h, respectively, denoting the time offsets, τ , applied to obtain the “shifted” quantity $F_s(\text{CRISSP})$. T_a and $T_a(t + \tau)$ are model air temperature inputs contemporary with, respectively, the $F(\text{meas})$ and $F_s(\text{CRISSP})$ curves in Figs. 4-7.

The most immediately apparent aspect of such comparisons was the previously noted (Marko et al., 2015a) shortfall of the SWIPS-derived $F(\text{meas})$ results from expectations based upon the simulated curves. The extent of this mismatch varied, very roughly, between 20:1 and 200:1 during the course of individual Intervals. The Marko et al. (2015a) estimate of 40:1 ratios were representative of comparisons between experimental and simulated peak values. Additional, comparably significant, differences were readily apparent in the basic characters of the $F(\text{meas})$ curves in Figs. 4-7 relative to their simulated counterparts. In the observational data, large changes in fractional volumes occurred both as functions of time during individual Intervals and in the nature of the variations associated with different Intervals. The time scales of variations ranged upward from a few to several hours, with observed initial peaks usually occurring 1 to 2 hours after the first appearances of suspended frazil. Post-peak behaviour showed sharp decreases of 50% to 80%. Intervals 2, 4 and 5 showed a classic single initial peak form, followed by extended periods of, relatively uniformly, low frazil content. Other Intervals (intervals 1 and 3) included multiple peaks separated by periods of low frazil content. All observed peaks rose and fell at rates comparable to those characteristic of the initial onsets of frazil Intervals. In the case of Interval 3 (Fig. 5), these variations spanned fractional volumes between, roughly, 1×10^{-5} and 5×10^{-5} . When averaged over the durations of individual Intervals, frazil contents were, typically, less than half of initial peak contents.

In contrast, the simulation results plotted in Figs 4-7 showed no evidence of frazil peaking phenomena. Instead the simulated initial sharp rises in fractional volume typically continued to

increase gradually until water temperatures rose above zero: suggesting a near-equilibrium balance of mass and energy exchanges. Fractional volume maxima were only attained several hours after the onset of supercooling. In sum, the simulations overestimated both the maximum values of water column frazil content (by almost two orders of magnitude) and the fraction of each Interval associated with comparable frazil presences.

Analysis of the thermodynamics of frazil initiation provides a quantitative basis for exploring the implications and origins of the simulation’s tendencies to over-predict frazil content. Such efforts provide insights into the mechanisms of river ice formation and can be framed within the context of the widely accepted, largely laboratory-derived, picture of the initial stages of frazil growth (Daly and Axelson, 1989) This picture assumes that, with constant water column heat loss, supercooling increases until nucleation is triggered and followed by rapid increases in frazil particle numbers and sizes through collision-driven secondary nucleation and growth. The consequent release of latent heat reduces supercooling, allowing water temperatures to slowly approach equilibrium levels. At the resulting temperature minimum, rates of heat loss are exactly balanced by latent heat production. Subsequent reductions in supercooling then require that the rates of latent heat release must exceed water column heat losses.

The thermodynamics of this situation are concisely captured by a characteristic heat flux ratio, defined as the ratio of the pre-initiation sensible heat flux, derived from the rate of change of water temperature, to the latent heat flux calculated from the initial rate of increase in water column frazil content. This ratio is internally consistent and relatively insensitive to a wide range of pre-initiation conditions. The fundamental requirement of this initiation model, that this ratio exceeds 1.0, provides an absolute standard of comparison for data evaluations which is independent of simulation details. Observations of lesser flux ratios are indicative of shortfalls in the energy balances which are an intrinsic part of the conceptual basis for frazil initiation as simulated by the CRISSP1D model.

Key data for assessing pre- and post-onset energy balances are compiled in Table 3 for Intervals 1-5 as derived from the CRISSP1D simulations and from the SWIPS and ADCP measurements. (Interval 2, listed in the Table, was omitted from earlier Figs. for space reasons, as it was of relatively short duration and characterized by $F(\text{meas})$ results similar to those of Interval 4.) The tabulated latent heat fluxes were calculated from $F_s(\text{CRISSP})$ results and from averages of $F(\text{meas})$ values derived from SWIPS data acquired 1.3, 2.6 and 3.6 m above the riverbed. The pre-onset listings include sensible heat fluxes calculated from water temperature time gradients, both as simulated and as deduced from ADCP T_w data. Measured sensible heat fluxes were not available for Interval 4, since, as discussed below in Section 4.2.2, $T_w(\text{meas})$ values held steadily at 0°C for approximately 90 hours prior to frazil onset.

Table 3. Listings of simulated and observed (measured and estimated) fluxes of sensible and latent heat. Ratios denote values of latent heat flux/sensible heat flux.

Interval	Simulated sensible heat flux (Wm^{-2})	Simulated latent heatflux (Wm^{-2})	Simulated ratio	Measured sensible heat flux (Wm^{-2})	Measured latent heat flux (Wm^{-2})	Measured ratio
1	445	751	1.69	162	8.9	0.055
2	252	665	2.64	233	11.0	0.055
3	489	1159	2.37	628	28.8	0.046
4	139	305	2.19	n.a.	17.7	n.a.
5	146	637	4.35	289	23.3	0.081

The simulated and measured sensible heat fluxes are seen to be of similar magnitude but show significant differences which do not appear to be correlated with the above-noted offsets in simulation timing. The corresponding average of the 5 simulated heat flux ratios, 2.6, is in line with a model of frazil initiation based upon laboratory results. Corresponding comparisons for the observed initiation periods show estimated latent heat fluxes falling short of the simulated quantities by almost two orders of magnitude. Specifically, the typical heat flux ratios of 0.05, are indicative of major shortfalls relative to the minimum value of 1.0 required by the principles underlying the simulations.

These shortfalls were deduced directly from rates of change in suspended frazil content as deduced from measurements made within the water column at frazil initiation. This timing rules out physical explanations in terms of processes which either alter surface heat loss rates or require time to develop. Two possible sources of low latent to sensible heat ratios are: physical removal of suspended frazil particles from the water column; and neglect of at least one major source of latent heat production. The CRISSP1D model already incorporates frazil removal by both buoyant rising of particles to the surface, and by their capture on the riverbed to produce anchor ice. However, neither of these processes adds additional latent heat to the water column. Moreover, Jasek et al (2011) demonstrated that both removal mechanisms required unreasonable rate coefficients to significantly lower frazil fractional volumes. Detailed calculations dismissing these possibilities for the 2011-2012 data sets were also presented in an Appendix).

The remaining and most plausible source of latent heat for frazil suppression is *in situ* anchor ice growth on the riverbed: the role of frazil capture being largely limited to the initial “seeding” of this growth. A key element in linking *in situ* growth to the observed frazil Intervals is that such Intervals were invariably initiated during periods of decreasing air temperature. This circumstance, when combined with the accumulated body of frazil and energy exchange data, suggests the following, relatively simple, scenario. Vigorous *in situ* anchor ice growth, triggered by small amounts of frazil deposition, reduces supercooling, thereby depressing frazil growth while simultaneously sustaining anchor ice production. The frazil intervals documented by SWIPS data are, thus, transient events, driven by intensifying atmospheric heat losses against a background of continuing *in situ* growth. Frazil production fades as the latent heat from the latter growth forces the system toward equilibrium. The transient nature of frazil events was, in some cases, also expressed by the presence of multiple prominent peaks in frazil content with each peak followed and/or preceded by longer periods of much lower frazil content. For Interval 4, which was immediately preceded by warm air temperatures and 90 hours of water temperatures between 0.00°C and -0.01°C, the onset of frazil growth coincided precisely with the start of such a period of falling air temperatures.

In situ anchor ice growth is not only required to make surface ice production rates consistent with low measurement-based water column frazil content estimates but, in addition, naturally accounts for the multiple-peak forms of frazil variability observed in some Intervals (see Figs. 4 and 5). Such variations in $F(\text{meas})$ are readily attributable to short-term reductions in latent heat input occasioned by buoyancy-driven release and upward transport of *in situ*-grown anchor ice. These reductions would re-initiate strong frazil growth by, effectively, re-setting water column conditions close to those which initially triggered frazil onset. The resulting new blooms of suspended frazil, typically appearing in the presence of decreasing air temperatures, would persist until increased latent heat production by renewed *in situ* growth again drives water column frazil contents down to lower levels. These oscillations would be critically dependent upon *in situ* freezing as a driving force. Specifically, multi-peaking could not occur if anchor ice growth proceeded primarily through frazil capture. Buoyant release of such ice would not “reset” conditions to be favourable for frazil formation since the only latent heat produced by such anchor ice growth would have entered the water column prior to frazil capture and incorporation on the riverbed. It should be noted that the 10 minute averaging of the SWIPS data dictates that the obtained estimates of F are representative of, roughly, 1 km

streamwise sampling regions. Oscillatory behaviour in such data is suggestive of synchronous anchor ice growth and release on relatively large spatial scales. It is also likely that there are random and quasi-continuous components of this upward anchor ice flux. Such transport was mimicked in the CRISSP1D simulations by the excessive concentrations of rising frazil required to reproduce observed levels of surface ice production.

It was not surprising that the most pronounced oscillations in water column frazil content occurred during Interval 3 (see Fig. 5) which coincided with the most prolonged and intense observed freezing event (Fig. 8b). The resulting, maximally rapid, anchor ice growth was likely to have shortened the time required for riverbed ice to thicken sufficiently to trigger buoyancy-driven release and transport to the river surface. Within this interpretation, sensitivities to cooling rates would appear to be most evident in the time dependences as opposed to the magnitudes of frazil fractional volume. The origins of Interval to Interval differences in frazil content time dependences will be examined in more detail in Section 4.2.2.

Within the context of linkages between changes in frazil content and degrees of supercooling, it is worth noting theoretical expectations (Daly, 1984) and observations (Osterkamp and Gosink, 1983) suggesting that reduced supercooling increases the particle sizes required for sustained frazil production. Evidence for this is presented in Fig. 9 in terms of changes in median effective particle radii at times coincident with peaking of fractional volumes during Interval 3 (Fig. 5). It can be seen that this measure of particle size (determined (Marko et al., 2015a) by SWIPS RUNSWIPS optimization of frazil population parameters) decreased during the peaking intervals before increasing again with subsequent decreases in supercooling and frazil content.

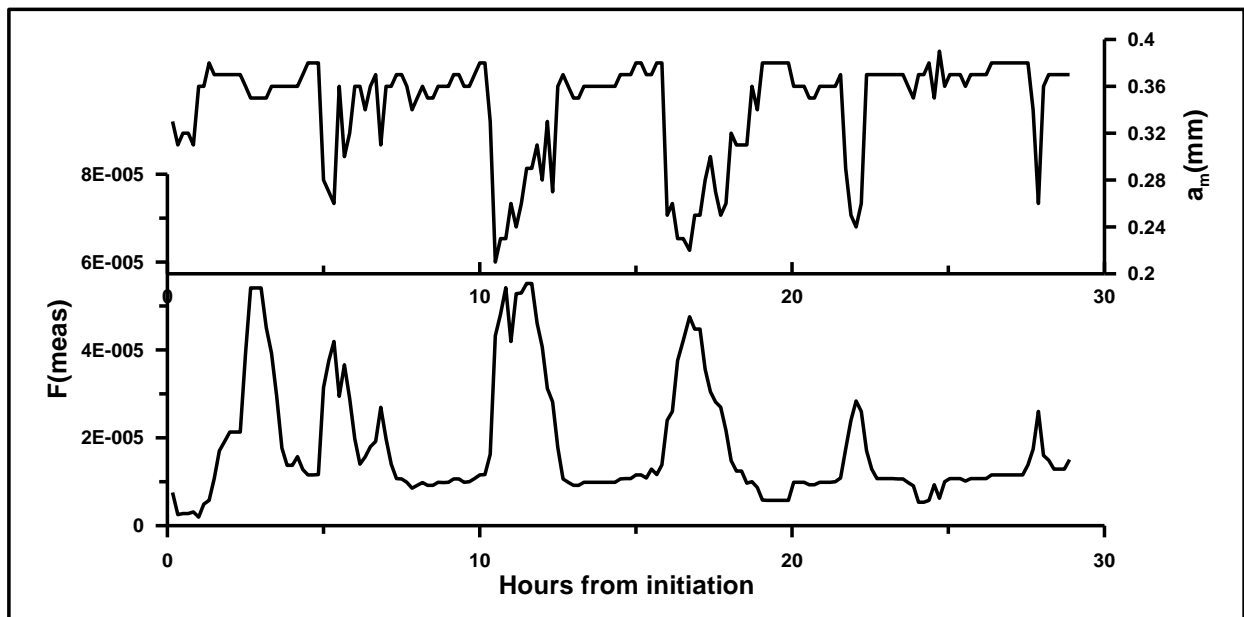


Fig. 9. Coincident variations in median frazil particle effective radius (a_m) and fractional volume ($F(\text{meas})$) during frazil Interval 3.

In concluding this Section, it is acknowledged that other, less quantifiable, explanations for multi-peaked fractional volume variations might be constructed in terms of unspecified stochastic river phenomena which locally introduce bodies of unexpectedly cold or warm water. Such possibilities provided impetus for seeking additional, more direct, signatures of *in situ* growth in Sections 3.2 and 4.

3.2 Relationships of ancillary water level data to anchor ice changes

Hydrostatic pressure data collected on the ADCP provided additional information on ice development through recognized connections (Beltaos, 2013) between anchor ice and water levels. Details of these connections are still ambiguous, especially in large regulated rivers subject to multiple sources of variability. Relevant water level variations were expected from river cross section and bed roughness changes which could be of either sign, depending upon the stage and location of anchor ice growth (Jasek et al., 2015). Ice impacts were detected by comparing measured water levels with expectations from ice-free CRISSP1D runs to account for flow travel times and attenuation of regulated dam discharges.

Such impacts are evident in the plot (Fig. 10) of “excess” water levels (Δ) at the SWIPS site: defined as differences between 10-point running averages of water levels derived from barometrically corrected pressure data and contemporary ice-free simulated values. Known periods of frazil production are indicated by the shaded areas in Fig. 10. The magnitudes of Δ were usually a few cm or less except within a day or so of frazil intervals when, prior to, roughly, Jan.15, excess water levels typically were on the order of 10 cm. Subsequently, $|\Delta|$ increased further, reaching and exceeding 0.5 m. Higher resolution plots of $\Delta(t)$, included in Figs. 4-7, show water level changes prior to and during the four depicted frazil intervals.

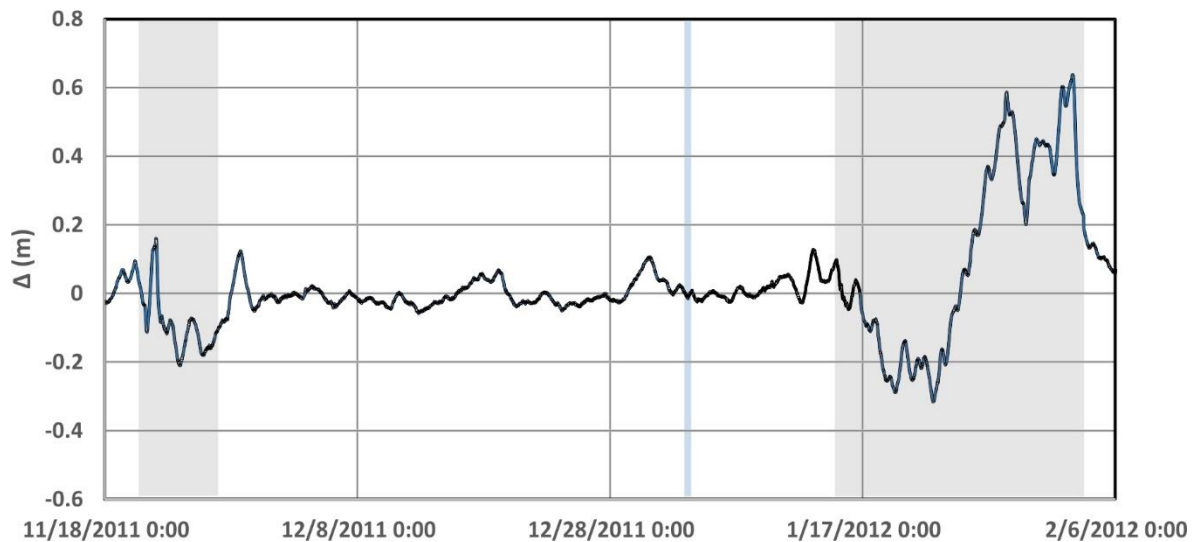


Fig. 10. Plot of differences, Δ , between 10 point running average ADCP water level estimates and CRISSP1D simulated water level estimates (at 30 minute intervals). Shading denotes timings of confirmed frazil presence. No attempt was made to document all frazil occurrences during the study period.

Two types of behaviour were apparent. Firstly, with Δ decreasing from peak values which either preceded (Fig. 4) or coincided (Fig. 5) with corresponding peaks in frazil content, and, secondly, with $\Delta(t)$ increasing almost monotonically increasing (Figs. 6 and 7). Although the number of observed events was small, rising water levels appeared to accompany the single-peaked form of $F(\text{meas})$ behaviour. This correspondence was particularly evident during the periods of low, relatively constant, $F(\text{meas})$ values associated (Section 3.1) with anchor ice accumulation and consequent changes in bed roughness and river cross section. Decreasing water levels were favoured during multiple-peaked intervals: most notably in Interval 3 where narrow $F(\text{meas})$ peaks were closely followed by visible $\Delta(t)$ counterparts (Fig. 5). Specifically, brief ice-related water level peaks occurred on the downslopes of peaks in local frazil content. Such timings are fully consistent with the interpretations of oscillatory $F(\text{meas})$ behaviour offered in Section 3.1. The peaks represent water level increases introduced by the “local” (i.e. within the sampling region) anchor ice growth which produced latent heat sufficient to reduce frazil contents below immediately preceding values. The

water level elevations produced by this growth were eventually dissipated by the contemporary large scale decreasing water level trend. The fading of local water level elevations during later portions of each low frazil content period could also be consistent with expectations (Kerr et al., 2002) that anchor ice roughness decreases with additional growth. It is also notable that the detectable “local” water level peaks were confined to Interval 3. This Interval was associated with both the season’s most intense cooling and included a period when the broader background of elevated water levels, which obscures contributions from small ‘localized’ peaks, fell to near-zero values.

In spite of these correspondences, local water levels, alone, appeared to offer only limited insights into anchor ice changes. This circumstance reflects the complexity of measured water level responses which are sums of positive and negative contributions from anchor ice processes often taking place simultaneously over broad upstream and/or downstream stretches of the river. For example, the observed appearances of rising water levels prior to local frazil detection could be evidence of downstream frazil and anchor ice growth altering upstream water levels without raising upstream frazil content. Alternatively, decreases in local water levels could arise from upstream increases in anchor ice volume and roughness which enhance water storage upstream of the monitoring site. In between these extremes, still other combinations of behaviour could occur.

4. Direct SWIPS characterization of anchor ice development and change

4.1 Impacts of anchor ice on SWIPS profiling results

Sections 3.1 and 3.2 presented at least two independent bodies of evidence for the dominant presence of anchor ice growth in early winter supercooling intervals. These data suggest that this growth occurs primarily *in situ*, probably reflecting the enhanced dissipation of latent heat enabled by the larger water velocity differentials attained adjacent to bottom-fixed- as opposed to free-drifting-ice surfaces (Petrovich, 1956). Similar conclusions on the dominance of *in situ* anchor ice growth in “deep” waters were previously drawn by Kempema and Ettema (2013) from morphological analyses of water intake blockages. However, it is important to note that none of the data presented thus far have provided information on the magnitudes or the spatial distributions of the inferred anchor ice growth. This lack reflects, in part, the “indirect” character of the acquired information: whereby anchor ice presence was invoked to explain variations in other environmental variables. The resulting knowledge gap is addressed below, more directly, using data on the impacts of ice on the SWIPS profile measurements.

This effort exploited the fact that the frazil studies of [Marko et al. \(2015\)](#) required careful setting of Interval 4 and 5 endpoints (Table 2) to avoid the anchor ice-induced acoustic beam blockages which terminated these Intervals. Similar blockages were not encountered earlier in the 2011-2012 season. The timings and intensities of the blockages, interpretable as two separate events, are summarized in Fig. 11 in terms of coarse severities as a function of time at each acoustic frequency. Three severity categories were delineated: unblocked, partially blocked and completely blocked. Partial blockages occurred during transitions between the unblocked (no obstruction) and completely blocked (no acoustic returns from the water column or river surface) extremes. Except for a three day February period separating the two events, additional data in Fig. 11 showed mean daily air temperatures remaining close to or below roughly, -5°C for times as late as Feb. 19 when the consolidated ice edge was 3 km upstream of the SWIPS.

The first event spanned the period between Jan. 26 and Feb. 3: with the onset of detectable obstruction progressing with time from higher to lower frequencies until blockage was complete in all four channels. A similar progression over the Feb. 7-19 period characterized the second event but complete blockages were limited to channels 1, 3 and 4.

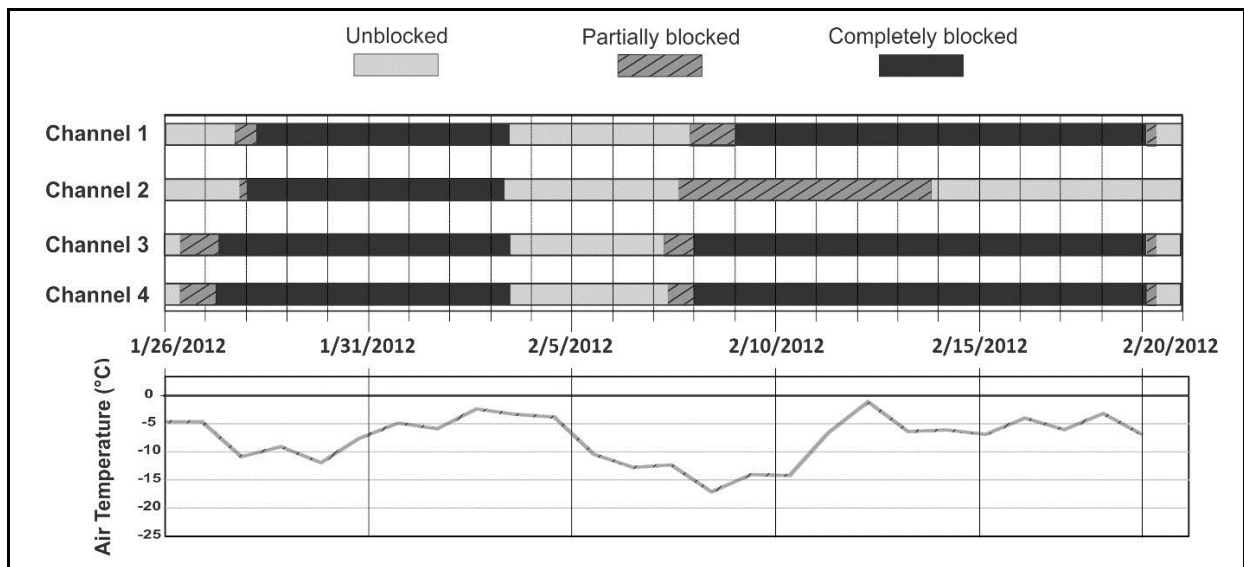


Fig. 11. Mean daily air temperatures at gauging station 7 km downstream from the SWIPS and the timings of observed acoustic beam blockages during the Jan. 26-Feb. 20, 2012 time period. The temperature data were confined to the period up to and just beyond the advance of the ice edge upstream of the SWIPS site. Uncertainties in blockage transitions were greatest (± 2 hours) at the starts and ends of partial blockages.

The principal features of SWIPS blockages are identified and interpreted for the first event in Section 4.1.1, with focus given to anchor ice-related issues. Section 4.1.2 provides an equivalent but shorter narrative on the second blockage event.

4.1.1 The first blockage event: Jan. 26-Feb.3, 2012

SWIPS data were characterized during all frazil intervals by strong, highly localized (in range), returns from the river surface, and weaker diffuse returns from frazil suspended in the water column. Both types of returns waxed and waned on time scales of seconds due to varying river surface conditions and frazil population changes. Such short term return variations can be assumed to be time-averaged by downstream drift, allowing variations over time in average return strength to be associated with sound attenuation by anchor ice on or immediately above the transducer faces. Such ice also produces changes in strong “close-in” returns (Jasek et al., 2005; Morse and Richard, 2009) from ranges immediately adjacent to the SWIPS (ranges < 0.5 m).

All identified constituents of SWIPS profiles are evident in the echograms of Figs. 12a,b which depict channel 4 and 1 data as, respectively, representative of high and low acoustic frequency results. Each echogram is a colour-coded display of digitized (in counts) backscattered signal voltages as a function of time corresponding to acoustic returns from targets at the indicated ranges from the transducers. Voltage data are actually acquired as a function of acoustic pulse travel time and converted into spatial ranges using the speed of sound in freshwater. Annotations in Fig. 12a highlight examples, in the most sensitive, high frequency, channel, of the three generic target types (river surface, suspended frazil and close-in).

Returns from suspended frazil were usually extinguished by anchor ice accumulations much smaller than required for detectable attenuation of surface target returns. This difference reflected the fact that detection of, typically weak, frazil targets requires high acoustic power levels, which, unavoidably, saturate contemporary surface target returns, rendering them insensitive to initial attenuation of incident power. Surface return weakening usually only becomes detectable after disappearance of frazil returns. This weakening is accompanied by observable increases in the range of the intense close-in returns which are always (i.e. independently of anchor ice presence)

associated with regions immediately adjacent to the transducers due to the finite “ring-down” times of transducers after pulse transmission.

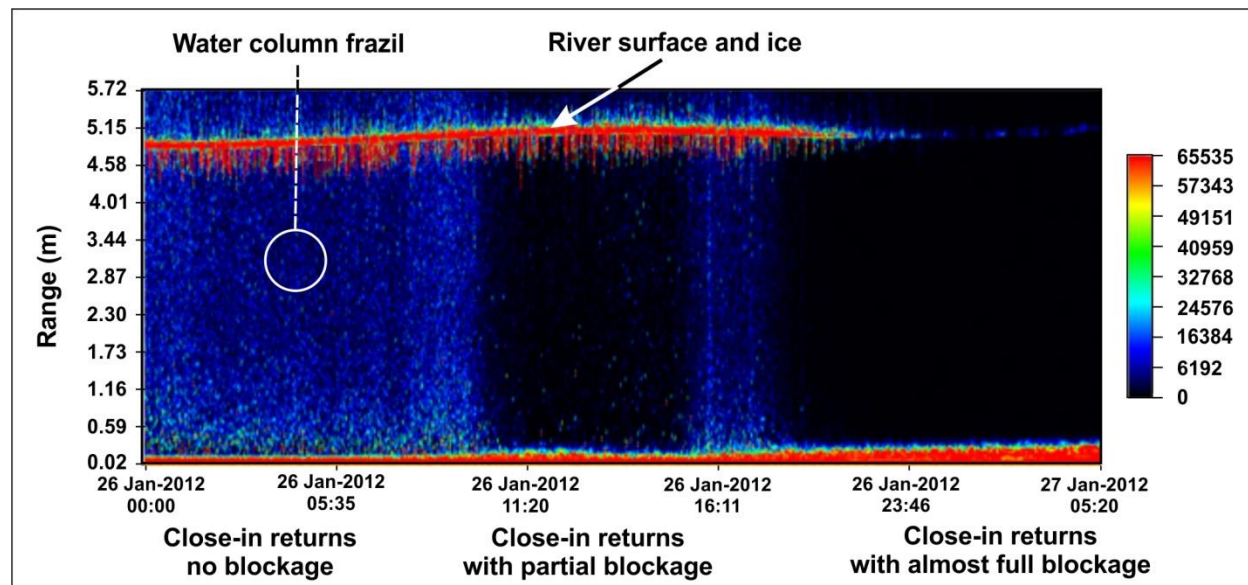


Fig. 12a. Echogram of the channel 4 (774 kHz) returns in the first blockage event.

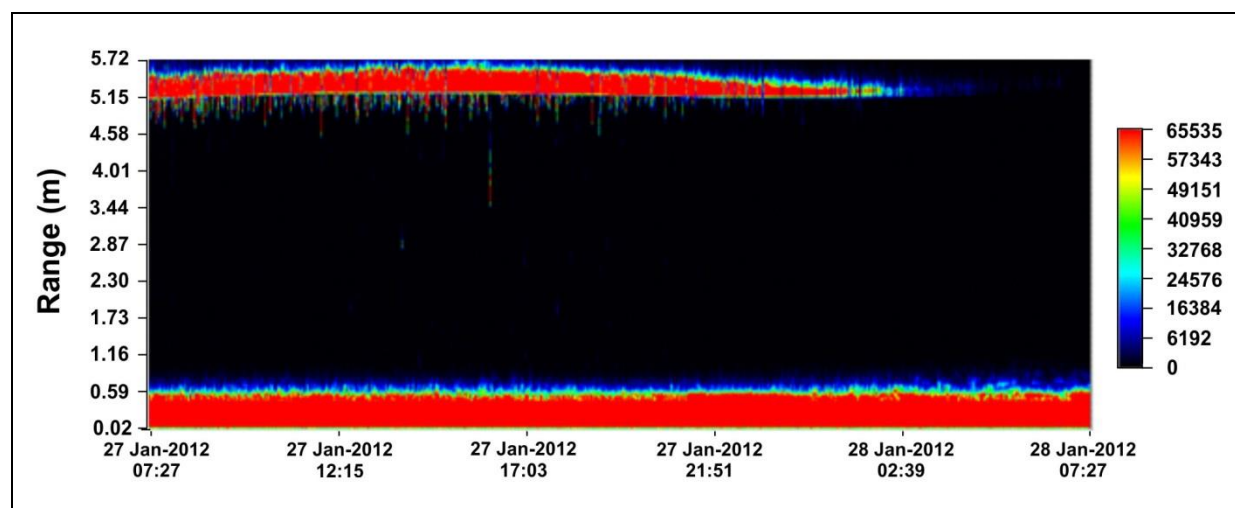


Fig. 12b. Echogram of the channel 1 (125 kHz) returns in the first blockage event.

In the first blockage event, backscattering by anchor ice was first detectable in close-in returns acquired in the two highest frequency channels at about 09:00 Jan. 26. Systematic channel to channel differences in the timing of both the first signs of surface signal fading and subsequent extinctions were readily apparent, first in the channel 4 (774 kHz) data (Fig. 12a), followed by successive later total losses of returns at progressively lower acoustic frequencies as depicted in Fig. 11. These differences reflect the tendency for attenuation to increase with acoustic frequency, raising the anchor ice growth threshold for producing detectable blockage at lower frequencies. This trend obscures the likelihood that, given the spatial proximity of the transducers, growth was initiated near-simultaneously in all channels.

The onset of blockages in channels 3 and 4 occurred, roughly, 15 hours after the Jan. 25 reappearances of water column returns immediately after a 14 hour period of negligible or very sporadic frazil presence. The 09:00, Jan. 26 blockage onset also coincided with the end of a notable gradual, very approximately 18 cm, rise in surface return range (indicative of the rising water levels

noted in Fig. 6). This onset was evident in: fading water column returns; increased maximum close-in return ranges; and in slight weakenings of the longest range components of saturated surface returns. The impacts of these blockages peaked at, roughly, 12:00 before diminishing until 18:00 when surface return strengths re-approached pre-blockage levels before retreating again about one hour later, coincident with strengthened close-in returns. Surface returns were undetectable by early morning, Jan. 27.

Evidence for blockage in channels 1 and 2 first appeared at, roughly, 18:00, Jan. 26 as very slight thickenings of the close-in returns, followed by fading water column returns and slow reductions in the spread of ranges associated with surface returns (Fig. 12b). As at higher frequencies, the latter changes featured preferential weakening and disappearance of later-arriving surface returns. This characteristic of surface returns, namely, the range stability of early-arriving signals, is employed below for quantitative data interpretation. Blockage impacts on these early returns were first evident at approximately 15:00, Jan. 26 when signal strengths fell slightly below the saturation level (65535 counts). Less subtle evidence for Channel 1 surface return blockage eventually appeared at times close to 00:00, Jan. 27 (Fig. 12b). Complete blockages of channel 1 water column returns occurred at 06:00, Jan. 28 or about 1 day after extinctions in the more attenuated high frequency channels.

Practical use of close-in data for anchor ice characterization was restricted to the two higher frequency channels associated with wavelengths short enough to justify the acoustic far field assumption (which allows neglect of interference effects introduced by the finite sizes of the transducer faces). The observed increases in maximum close-in return range provided a basis for estimating anchor ice thickness on transducer faces. Unfortunately, the relationship between this thickness and the vertical extent of the close-in target portions of the echogram breaks down when the attenuation becomes large enough to preclude detection of returns from the upper reaches of the blocking layer. Further accretion, then, has little impact on maximum close-in return ranges but, instead, introduces hard to interpret changes in returns from lower, still insonified, portions of the ice layer. This levelling off and change in character is evident in Figs. 13a,b which show zoomed-in channel 4 close-in returns during two 13 h periods subsequent to surface return extinction in this channel.

The first of these intervals (Fig. 13a) began at 06:00, Jan. 27, roughly coincident with channel 4 surface return extinction. The second depicted interval (Fig. 13b) started 24 hours later at 06:00, Jan. 28 coincident with the first signs of equivalent surface return extinctions in the low frequency channel 1. The effects of additional ice accumulation over the intervening period are evident primarily as “textural” changes in longer range channel 4 close-in returns. Specifically, higher temporal frequency components of variability in the upper portions of these returns are significantly reduced in Fig. 13b relative to observations in the earlier period (Fig. 13a). This change (equivalent to low-pass filtering) was attributable to the additional ice accumulations required to extinguish SWIPS surface returns at the lower, and less severely attenuated (Langleben, 1969), channel 1 frequency. The resulting reduction in short timescale variability suggests that this accretion increased physical stability in the acoustically detectable portions of the anchor ice layer. Further evidence for relationships between layer stability and close-in variability will be introduced below in data collected during clearance of this blockage.

The weak sensitivities of close-in returns at low acoustic frequencies to anchor ice accumulation are due to the correspondingly greater duration of transducer ringing and the persistence of near-field scattering conditions out to larger ranges. Although this insensitivity precluded use for ice thickness estimates; the maximum ranges of such returns did increase progressively throughout the course of the blockage event: levelling off after, approximately, 12:00, Jan. 28. As noted at higher acoustic frequencies, close-in return data acquired at subsequent times were compatible with continued anchor ice accretion above the SWIPS transducers. Taken together, all acoustic data suggest that

anchor ice was accumulating on the surface of the SWIPS instrument between 10:00 Jan. 26 and no earlier than 12:00, Jan. 28: a period of 50 hours. As indicated in Fig. 11, observations showed anchor ice sustaining complete acoustic blockages until Feb. 3.

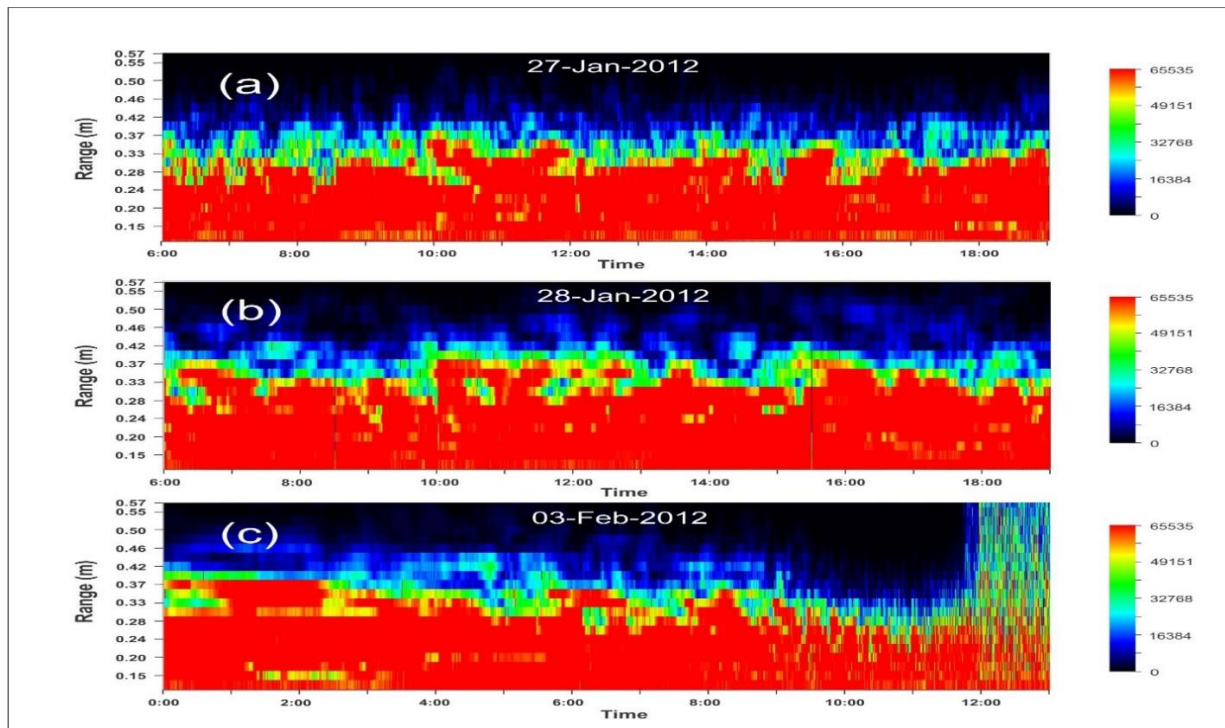


Fig.13. Zoomed-in channel 4 close-in returns acquired during 13 h intervals at different stages of the first blockage event. Panels a) and b) depict intervals initiated at times coinciding with complete extinctions in, respectively, the high (06:00, Jan. 27) and low (06:00, Jan. 28) frequency channels, roughly 24 and 48 hours into the event. Panel c) displays channel 4 data initiated at 00:00, Feb. 3, spanning ice clearance at the end of the blockage

Subsequent clearances were sudden in all channels as illustrated by the Channel 4 and 2 data of Figs. 14a,b, respectively: occurring more than a full day after a long run of daily supercooling conditions (Fig. 10). Simultaneous recoveries of profiling capabilities were particularly notable in the three channels (1, 3 and 4) associated with immediately adjacent transducers. These recoveries, illustrated by the high frequency, channel 4, echogram of Fig. 14a, were delayed by about 3.5 hours relative to channel 2 (Fig. 14b). This delay offered initial evidence of possible recent heating and/or flow condition changes at the isolated, separately mounted (Fig. 1), channel 2 transducer.

The channel 4 data of Fig. 14a also illustrate an important feature of the close-in higher frequency returns at times leading up to blockage clearances. This feature is more clearly evident in a zoomed-in view of portions of this data (Fig. 13c) acquired during the 13 hour period immediately preceding clearance. Progressive layer thinning and increasing higher frequency variability are evident throughout, at least, the last 10 hours of this period. Such changes suggest an extended period of anchor ice degradation and destabilization preceded the sudden Feb. 3 clearance and recovery of SWIPS capabilities.

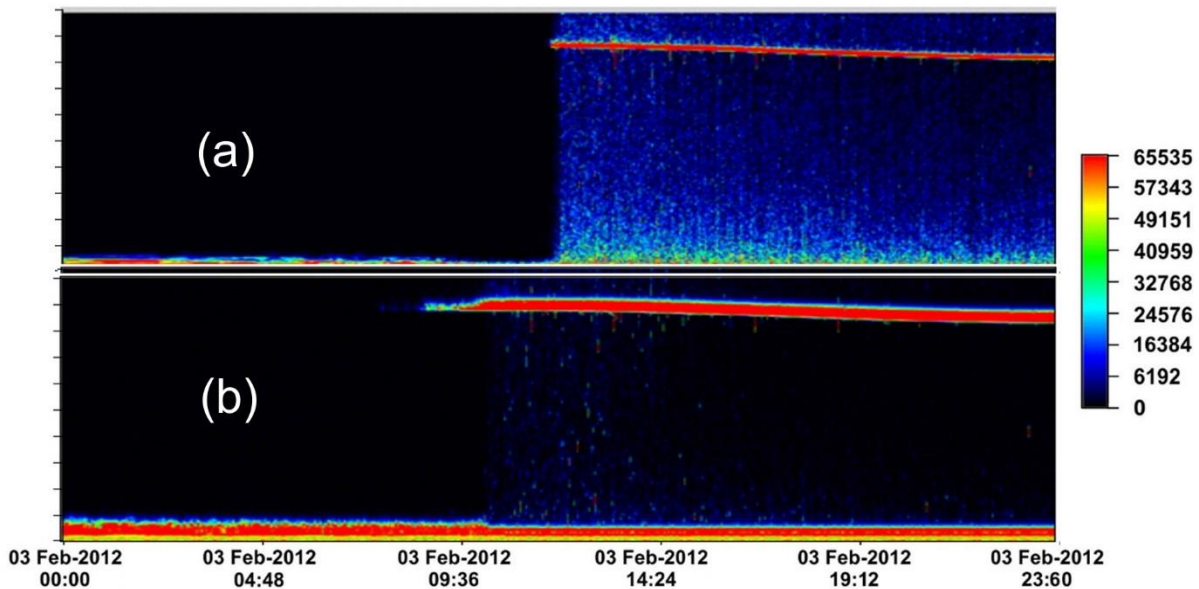


Fig. 14. Echograms of (a) the channel 4 (774 kHz) and (b) channel 2 returns detected leading to and following clearances of anchor ice accumulated during the first blockage event.

4.1.2 The second blockage event: Feb. 3-Feb. 19, 2012

The distinctive nature of channel 2 data at the end of the first blockage event was even more apparent after the, roughly, 00:00, Feb. 7 start of the second blockage event (Fig. 11) which extinguished returns in all other channels. Total blockage was first achieved in channel 4 around midnight, Feb. 7, followed, about 24 hours later, by channel 1 extinction. As in the earlier event, roughly 8 hour sequences of partial blockages and clearances in channels 4 and 3 were followed by renewed and intensifying blockages and, eventually, by complete extinctions. In both events, channel 1 extinctions occurred during midnight hours, roughly, one full day after channel 3 and 4 extinctions. High frequency close-in return data showed evidence of ongoing changes subsequent to the Feb. 9 channel 1 extinction, indicative of another long run of continuous SWIPS blockages. Definitive clearances did not occur in channels 1, 3 and 4 until Feb. 19 when multiple ground observers reported the consolidated ice edge becoming established 3 km upstream of the SWIPS site. In channel 2, weakened surface returns, indicative of blockage onset, only appeared on, Feb. 9 before strengthening again on Feb. 11 just prior to the ice edge shifting to within 600 m of the SWIPS.

A notable feature of the second (February) mid-day partial blockage (08:00-13:00, Feb.7), was the appearance (Fig. 15), immediately after blockage clearance, of small but significant numbers of highly localized (in time and space) targets scattered throughout the water column between, roughly, 14:00 and 17:00, Feb. 7. These targets, confined to individual pings, were characterized by mid- to near-maximal strength values (yellow to orange false colours) which well exceeded those associated with the great bulk of contemporary water column returns. Such features were not observed in periods immediately following high frazil concentrations and renewed SWIPS blockages. The character of these targets was consistent with expectations from large rising ice fragments associated, in Section 3.1, with anchor ice clearance.

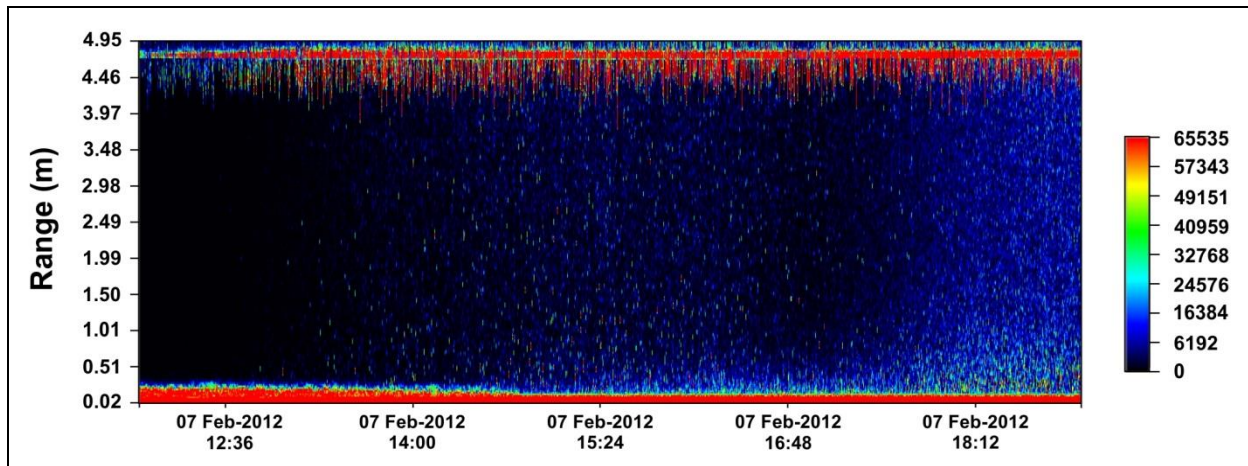


Fig. 15. An Echogram depiction of the last stage of the initial, partial, fadeout of Interval 5 channel 4 SWIPS returns. Anchor ice clearance began at about 13:15 followed at 18:00 by reappearances of high concentrations of water column frazil presaging later anchor ice regrowth and water column and surface signal extinction. Detection of localized medium- and near-maximum-strength water column returns (yellow-orange colour-coded) at times between 13:00 and 17:00 was consistent with presence of released anchor ice fragments.

4.2 Extracting and interpreting anchor ice information from SWIPS blockage data

The above results suggest that anchor ice was an almost continuous presence on the SWIPS instrument over a nearly four week period immediately preceding local ice consolidation. The relationship between this presence and the spatially extensive body of riverbed anchor ice deduced in Section 3 from frazil and water level data remains to be established. This effort begins in Section 4.2.1 with quantitative estimates of anchor ice accumulations on the SWIPS transducers. Such estimates provide a basis for using earlier results and interpretations to construct (in Section 4.2.2) a defensible conceptual model of the changes which occurred at and around the SWIPS instrument prior to surface ice consolidation.

4.2.1 Anchor ice accumulation on the SWIPS instrument

Quantifying ice accumulation on the SWIPS instrument was complicated by a lack of data on the effectiveness of the applied heating as well as by limited knowledge of anchor ice properties such as porosity, intrinsic sound speed and rates of sound attenuation relevant to interpreting SWIPS data. The heating uncertainty effectively limited estimates to minimum values of ice thicknesses and accumulation rates. Sound speed information was sought by establishing bounds on possible values, utilizing both an above-noted feature of partially blocked surface signal returns and earlier estimates of sound speed in similar ice forms. The sound speed requirement reflected the fact that the maximum time delay associated with close-in returns (derived from ice-induced increases in the maximum ranges of these returns) is equal to twice the thickness of the anchor ice divided by its mean intrinsic sound speed. As noted above, this approach was applicable only when significant returns were detectable from regions above the anchor ice. This restriction assured full ice layer sampling but confined measurements to periods when maximum close-in return ranges were increasing or decreasing with time.

Uncertainties in estimating differences between the speed of sound in, alternatively, anchor ice and 0°C freshwater can be linked to corresponding uncertainties in the observed, nominally unchanging, ranges of surface returns during periods of partial blockage.

Specifically anchor ice, of thickness d , alters the apparent range, r , of the first-arriving surface returns by:

$$\Delta r = ((c_w - c_a)/c_a)d, \quad [2]$$

where c_w and c_a are the speeds of sound at 0°C in, respectively, freshwater and anchor ice. Reasonable minimum estimates of sound speed in anchor ice were available from earlier, 1000 ms^{-1} and 1200 ms^{-1} , determinations made in, respectively, crude laboratory- and Peace River field-measurement programs carried out on slush ice (Marko and Jasek, 2010a). A more robust, if less applicable, extreme upper limit was given by the 3840 ms^{-1} value measured by Vogt et al. (2008) in bubble-free zero porosity ice. These results were used to set 1000 ms^{-1} and 1800 ms^{-1} as possible lower and upper bounds of anchor ice sound speed. Insertion of these values into Eq. 2 suggested that anchor ice growth would have, respectively, altered the apparent range of surface returns r by +40% and -22% of the blocking ice thickness. For a 20 cm anchor ice layer, these shifts, +8 cm and -4.5 cm, respectively, fell outside of the estimated, +/-4 cm, uncertainties in our observations of blockage-independent surface return ranges. By implying that $1000 \text{ ms}^{-1} \leq c_a \leq 1800 \text{ ms}^{-1}$, these results allowed us to equate c_a to the intermediate 1402 ms^{-1} speed of sound in 0°C water without introducing errors in excess of +/-30%. This choice, conveniently, enabled maximum close-in range values (and, hence, anchor ice thicknesses) to be read directly off the echogram plots with tolerable accuracy.

To minimize complications from wavelength-sensitive near-field effects, applications of this method were restricted to data acquired at the highest acoustic frequency (channel 4) characterized by minimal near-field spatial extents. Estimates were derived during each blockage event from changes in maximum close-in ranges relative to values observed immediately prior to detectable range increases. Estimation was terminated when no additional increments in maximum range were detected. In both events, temporary partial blockage clearances (noted in Section 4.1) were ignored, restricting estimates to differences between successively larger observed maximum return ranges relative to pre-blockage values. The extracted thicknesses, derived from shifts in maximum ranges associated with counts > 24000, are plotted in Fig. 16 as a function of time after each blockage onset.

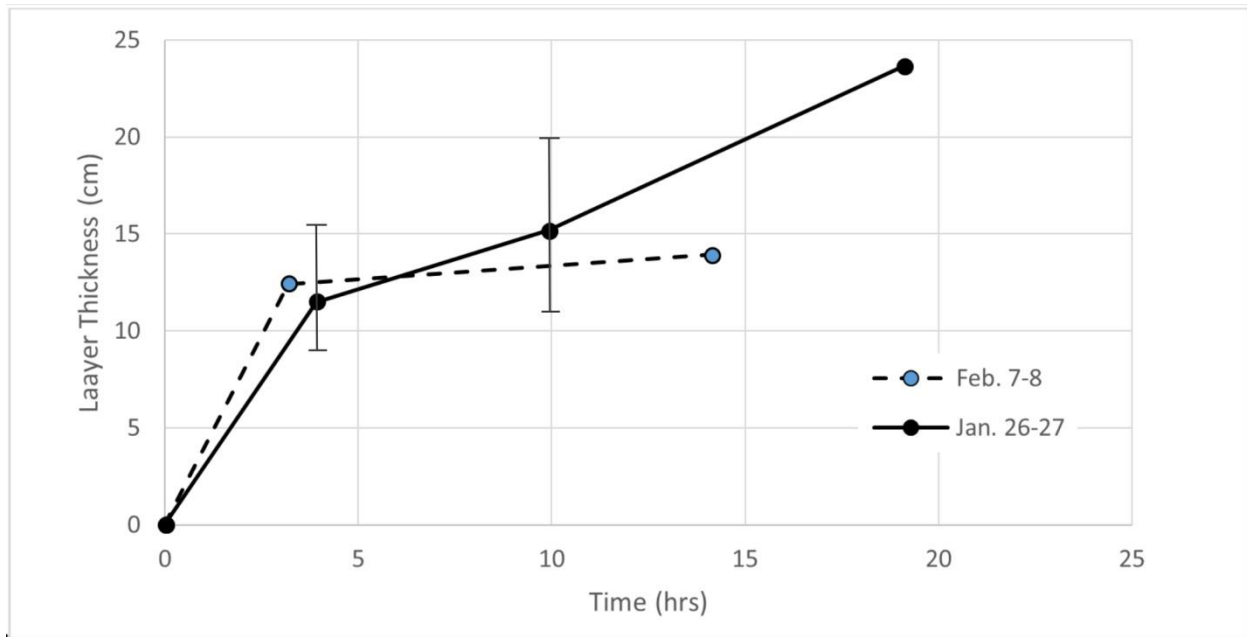


Fig. 16. Anchor ice accretion estimates during the Jan. 26-27 and Feb. 7-8 blockage events as a function of time since event onset. The error bars on the Jan. 26-27 data are representative of all estimates.

While probably underestimating actual thicknesses, our choice of a moderately high count threshold minimized possibilities for overestimation by inclusion of late returns from multiple scattering. The plotted results showed detectable accumulations reaching 23 cm and 14 cm during, respectively, the first and second blocking events. Roughly similar, 3-4 cmh⁻¹, growth rates characterized the initial stages of both events (i.e. prior to temporary clearing). Averaged over the measureable portions of both events, layer thicknesses increased at approximately 1 cmh⁻¹. These growth rates are well beyond levels sustainable by frazil capture-based anchor ice production (Marko et al., 2015b): again, supporting *in situ* process dominance.

4.2.2 Anchor ice on the SWIPS and in the surrounding environment: inter-relationships

The evidence for anchor ice growth presented earlier in this Section is based solely upon observations made upon ice accreted on the SWIPS transducers. No data were acquired directly linking this ice to the anchor ice presence indirectly inferred, in Section 3.1, from much larger bodies of frazil content-, energy balance- and water level-data acquired at the SWIPS site. Those data and the accumulations detected on the heated, elevated and attachment-resistant SWIPS surfaces would appear to require that comparable or greater ice accumulations occurred on the nearby riverbed during each frazil Interval.

In supporting this point of view, quantitative relationships were sought between anchor ice on the SWIPS instrument and concomitant riverbed growth during the two observed blockage Intervals. This effort drew upon an earlier anchor ice study carried out in a laboratory flume (Qu and Doering, 2007). In that work, frazil was seen to initially collect and build up in the interstices of boulders: eventually forming, through frazil capture and, possibly, *in situ* growth, a bottom-covering ice layer identified as “anchor ice”. A notable feature of this ice was that it advanced by “flowing” over higher downstream obstacles. Within this picture, onsets of SWIPS blockage could be seen as requiring thickening or growth of anchor ice on the adjacent riverbed to a height comparable to that (29 cm) of the elevated transducer surfaces. Further growth would initiate overflow and SWIPS blockage. This process readily lends itself to reproducing the two-step character of the two blockage events, whereby initial weakening of water column and surface target returns was followed by a brief recovery and, then, by final fade out and extinction (see Fig. 12a) of returns from the water column above the anchor ice layer. The temporary recoveries would have been driven by mid-day solar fluxes which produce melt-backs and partial clearances. Renewed weakening and eventual extinction of returns would follow with further supercooling and resumed overflow. It is possible that equilibrium in the presence of applied heating allowed “bridges” of riverbed ice to span but not make direct contact with heated transducer faces.

This, probably oversimplified, picture provided a reasonable basis for establishing quantitative connections between transducer blockage and nearby riverbed ice growth. Such connections were most unambiguously accessible from data gathered during Interval 5 which was immediately preceded by a 72 hour period characterized by undetectable water column frazil and simulated and ADCP-measured water temperatures as high as 1.1°C and 0.5°C, respectively. Under those conditions, the growth of the anchor ice which terminated Interval 5 could be assumed to have begun on an ice-free riverbed at the 00:00, Feb. 7 onset of frazil growth, roughly 8 hours before the first signs of subsequent blockages. The latter delay was assumed to be associated with accumulation of the 29 cm layer of riverbed ice required to initiate transducer overflow and subsequent impacts upon acoustic detection. The resulting average growth rates of 3.5 cmh⁻¹ were similar to rates estimated in Section 4.2.1 for anchor ice accumulation on the SWIPS transducers during subsequent blockages. CRISSP1D cumulative heat fluxes were calculated relative to frazil onset for this Interval using contemporary CRISSP1D environmental data inputs (i.e. corresponding to T_a(t) in Fig. 4d). Plots of these results (along with re-plots of T_a) in Fig. 17a show blockage onset at the end of this Interval (denoted by shading), coincided with a cumulative flux of 7.2 MJm⁻².

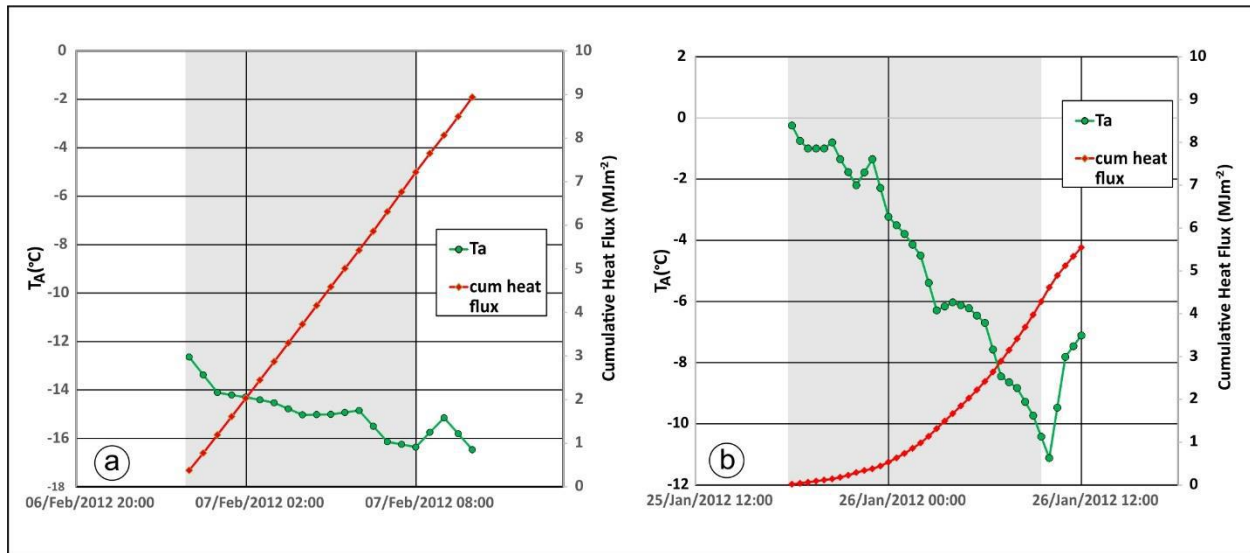


Fig.17 Plots of CRISSP1D air temperature inputs and unshifted cumulative heat fluxes for: a) Interval 5 and b) Interval 4. Shaded regions denote interval timings and duration. Cumulative fluxes were computed relative to the start of each frazil Interval as denoted by shading. Values of these fluxes at the onsets of blockages occurring at the end of each Interval (i.e. at the right hand boundaries of the shaded regions) were, respectively, 7.2 and 4.3 MJm⁻². Air temperatures during the first 3.5 h of Interval 4 were manually decreased from their above zero values to be compatible with the observed presence of water column frazil and supercooling.

of this methodology to Interval 4 were complicated by considerable ambiguities in prevailing riverbed and water column conditions during the, roughly, 17 h period which separated the onset of this Interval from the, approximately, 00:00, Jan 25 end of a long period of frazil and anchor ice growth. The problematic period was marked by: inclusion of model air temperature inputs which rose above 0°C; measured water temperatures between +0.01°C and -0.01°C; and evidence of low but measurable water column frazil contents. The latter frazil features were concentrated in the lower water column at times less than 3 hours prior to Interval onset. In fact, plots of the contemporary and immediately preceding CRISSP input air temperatures (Fig. 4c) showed above-freezing temperatures at that onset. It is reasonable to conclude the latter air temperature inputs were unreasonably high, at least at the beginning of this Interval, and that, frazil growth began in the presence of a significant remnant layer of anchor ice. This presence would account for the observed stability of near-freezing T_w values during a period of rising air temperatures. More importantly for our purposes, this layer would have slightly lowered requirements for the cumulative heat losses and additional anchor ice growth needed to initiate overflow and subsequent SWIPS blockages. This possibility is consistent with blockage onset occurring (Fig. 17b) at a cumulative heat flux value which was, roughly, only 63% of that required for the Interval 5 blockage even after T_a values at the beginning of the Interval were manually adjusted downward to avoid unphysical supercooling onset at air temperatures > 0°C. These interpretations of Interval 4 and 5 data are consistent with water level rises observed (Section 4.1.1) immediately prior to the subsequent blockages (Fig. 12a) and evidence for anchor ice layer growth with thicknesses ≥ 0.5 m comparable to contemporary late January and early February water level changes (Fig. 10).

Quantitative linkages between latent heat fluxes and rates of anchor ice growth prior to blockage onset offered additional insights into riverbed anchor ice properties utilizing the assumption that blockage onset required prior buildup of a 29 cm anchor ice layer. The 7.2 MJm⁻² cumulative heat flux threshold associated with this requirement (derived from the least problematic Interval 5 data) would have produced ice mass growth equivalent to, approximately, 21 kg m⁻², corresponding to an ice layer with a porosity of 92%. While such an estimate would justify our assumption, in Section

4.2.1, of negligible deviations from freshwater sound speed, it also may be inconsistent with earlier (Marko and Jasek, 2010a) observations of drastic anchor ice impacts on deployed instruments. It is also outside of the 71%-84% range of porosities estimated (Parkinson et al., 1984) for St. Lawrence River anchor ice grown at air temperatures $-5^{\circ}\text{C} \leq T \leq -25^{\circ}\text{C}$. Both sets of estimates exceeded, by more than a factor of 2, the porosity ranges reported by Dube' et al. (2013). Although associated with accretion rates, 0.5 to 3.5 cmh^{-1} , comparable to those deduced from our data, the Dube' et al. (2013) estimates were made at room temperatures on small, heterogeneous, samples collected in steep small river environments using CAT Scan techniques. Such differences complicated easy cross-comparisons. It is also possible that our high porosity values reflect use of heat fluxes in anchor ice-free simulations "tuned" to reproduce observed surface ice parameters. The resulting value of $K = 17 \text{ Wm}^{-2} \text{ }^{\circ}\text{C}^{-1}$, was outside the 20 - $60 \text{ Wm}^{-2} \text{ }^{\circ}\text{C}^{-1}$ range suggested (Shen et al., 1984; Prowse, 1987) for St. Lawrence River conditions. An alternative, mid-range, choice of $40 \text{ Wm}^{-2} \text{ }^{\circ}\text{C}^{-1}$ would have increased the minimum cumulative heat flux requirements to approximately 15.1 MJm^{-2} , lowering our porosity estimates to 84% which is at the upper end of the Parkinson (1984) range.

Our use of heat flux estimates to link SWIPS instrument- and adjacent riverbed- ice also provided a means of explaining the most striking oddity encountered in our study, namely, the absence of SWIPS blockages prior to Jan. 26. Such absences, at least initially, appeared to be inconsistent with the inferred (Section 3.1) growth of anchor ice during all observed frazil Intervals and the fact that the season's most intense supercooling events occurred during this earlier, blockage-free, period. Explanations in terms of the Froude Number threshold suggested by Kerr et al. (2002) were found to be inconsistent with the fact that sub-threshold conditions prevailed throughout the entire pre-consolidation period. Our observations were found to be explicable, however, when the simple ice overflow model was combined with previously suggested (Section 3.1) connections between anchor ice stability and the characteristic time dependences of frazil fractional volume variations.

Only one of the three Intervals in the blockage free period, Interval 2 (Jan. 3,) exhibited the classic single peak form of $F(\text{meas})$ data common to the two observed blockage-producing Intervals (see Figs. 6 and 7). This Interval shared further commonality with Interval 4 in that frazil growth occurred under similarly moderate, -5°C to -10°C , air temperatures. Nevertheless, the computed cumulative heat flux over the full 6 hour duration of the Interval yielded a value, 2.8 MJm^{-2} , which was well below the 7.2 MJm^{-2} threshold assumed to be required for initiating SWIPS blockages. The other two blockage-free Intervals 1 and 3, on the other hand, were readily distinguishable from all other studied Intervals. Specifically, these Intervals exhibited the previously noted (Section 3.1) multi-peaked $F(\text{meas})$ time dependences and occurred in the presence of significantly lower (-16.5°C to -19°C and -14°C to -22°C , respectively) air temperatures (T_a) (Figs. 8a,b). Cumulative heat flux computations indicated that heat flux blockage thresholds should have been exceeded 7 h (Interval 1) and 6.5 h (Interval 3) after corresponding initial frazil onsets. Since additional peaks began to appear in these Intervals 3.7 and 4 hours after corresponding onsets, absences of blockages were consistent with the prior thinning and clearance of riverbed anchor ice suggested (Section 3.1) to have preceded peak occurrences. These reductions of layer thickness effectively short-circuited ice overflow onto the SWIPS surfaces, precluding blockage¹.

Although we have neglected other potential influences on anchor ice stability such as seasonally varying riverbed heat fluxes, the most salient implication of the frazil profile and SWIPS blockage results is that the physical stability of riverbed anchor ice is extremely sensitive to atmospheric cooling rates. Thus, anchor ice formed under "hard" freezing conditions, i.e. air temperatures below,

¹ It is to be noted that the procedure used to characterize early season blockage probabilities is insensitive to uncertainties in the coefficient, K , since blockage prospects were evaluated using a common threshold established from Interval 5 data. Consequently, adjustments in K would only change the ice mass threshold for blockage onset: leaving, unaffected, prior conclusions on threshold exceedance.

very roughly, -15°C , was much less likely to remain in place relative to ice grown at higher temperatures (“soft” freezing conditions). This situation is schematically depicted in Fig. 18. The suggested correspondence is not inconsistent with Parkinson’s (1984) early work which identified physical differences between anchor ice grown at, alternatively, air temperatures between -5°C and -10°C and near -20°C . Similarly, the physical stabilities of ice dams containing anchor ice were noted (Dube’ et al., 2013) to increase when grown during multiple intervals of modest cooling as opposed to single episodes of “hard” freezing conditions.

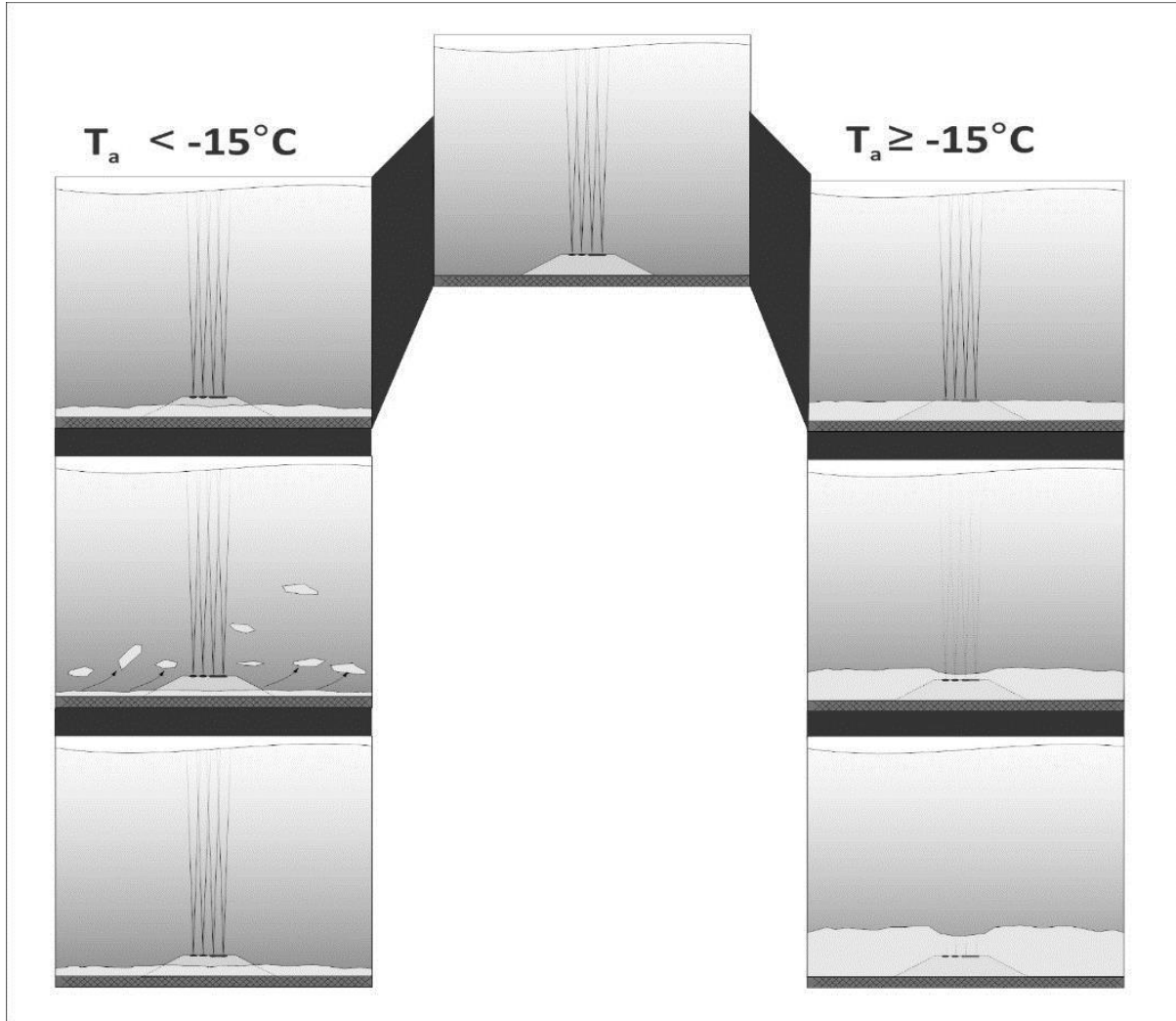


Fig. 18. Schematic illustrations of impacts on SWIPS profiling of proposed anchor ice layer evolution under alternatively soft ($T_a \geq -15^{\circ}\text{C}$) and hard ($T_a < -15^{\circ}\text{C}$) supercooling conditions.

5. Summary, Conclusions and Recommendations

5.1 Summary and Conclusions

Detailed analyses of SWIPS profile and ancillary river and environmental data were used to clarify the origins of over-predictions of Peace River frazil content by a model which excludes anchor ice growth. It was found that frazil fractional volume magnitude and time dependence data were only explicable in terms of *in situ* anchor ice growth throughout all supercooling intervals. The principal role of the extremely low concentrations of frazil detected was inferred to be the seeding of such anchor ice growth by physical capture on the riverbed. The observed sharp time-variations in frazil content during individual frazil intervals spanned almost an order of magnitude and, yet, even peak levels were almost two orders of magnitude below model predictions. Changes during supercooling intervals appeared to be sensitive to cooling rates which controlled attainable anchor ice thicknesses

and stabilities: with greater (lesser) cooling rates giving rise to more (less) frequent transfers of anchor ice to the river surface. SWIPS profile data showed direct evidence of such transfers, in the form of strong, highly localized (in space and time), water column targets consistent the presence of destabilized anchor ice fragments.

Water level changes induced by riverbed anchor ice were detected prior to and during frazil Intervals. Such changes spanned all supercooling periods but began to increase markedly in strength in late January. Most of these changes, detected in the absence of significant frazil at the monitoring site, were indicative of contributions from non-local anchor ice growth. Definitive detection of distinct local anchor ice impacts on water levels were confined to a single frazil Interval associated with the season's most intense cooling event and minimal water level impacts from non-local anchor ice.

Observations of anchor ice layer thicknesses large enough to obstruct SWIPS profiling were in accord with a simple conceptual model whereby the riverbed anchor ice layer progressively thickens and, eventually, overflows onto SWIPS measurement surfaces. Expectations from this model, which is driven by heat losses to the atmosphere, matched variations in detected suspended frazil content and in the observed timings of SWIPS blockages relative to supercooling onsets. This model allowed estimation of riverbed anchor ice growth rates, on the order of $1\text{-}4\text{ cmh}^{-1}$, which were comparable to rates independently deduced from accumulations on the SWIPS instrument. Such accumulations were estimated to attain thicknesses at least as large as several tens of cm. Ice growth rates on the riverbed and their Interval to Interval variations were consistent with heat losses proportional to differences between atmospheric- and water temperatures. Crude estimates of anchor ice porosity yielded values above or at the upper end of the 71-84% range previously estimated by Parkinson (1984). Overall, given the frequencies of supercooling events and the inferred frazil and riverbed ice growth rates, *in situ* anchor ice was identified as the dominant immediate source of surface ice mass. This conclusion is contrary to long held and ongoing (U. of Alberta, 2015) assumptions that the bulk of surface ice growth is attributable to surfacing water column frazil. Our confidence in the opposing view reflects both the robustness of the frazil content estimates (see Section 2) and the availability of independent verification in terms of calibration-insensitive details of SWIPS profiles and unique water level variations.

5.2 Recommendations

In our view, the principal significance of this work lies in its implications for future directions of ice monitoring and research in medium- and larger-sized rivers. The results suggest that new measurements and modelling advances are needed to further clarify and quantify relationships among key, generically different, river ice constituents. At present, only surface and frazil ice can be considered to be relatively "monitorable" constituents. Anchor ice, as a proposed major player in river ice growth, poses new challenges for systematic quantitative treatment. The SWIPS acoustic measurements represent large scale spatial averages of suspended frazil content, and in combination with a relatively unsophisticated temperature sensor, yield broad insights into the overall energy balance of ice formation. Clearly improved description and forecasting of changes in surface- and frazil-ice conditions require additional knowledge linking these ice forms to anchor ice processes. This may necessitate near-simultaneous studies of contemporary frazil and anchor ice changes as functions of water depth, atmospheric parameters, flow velocity, radiative fluxes, riverbed composition and time. Measures of anchor ice spatial extents, thicknesses, porosities, crystal sizes and mechanical strength are of particular interest. At a minimum, such data could quantify the suggested (Kempema and Ettema, 2015) different environmental dependences of the alternative *in situ* and frazil capture mechanisms for anchor ice production.

Emphasizing simultaneous acquisition of anchor-, frazil-, and surface-ice data anticipates that the latter two ice forms will continue to be most accessible to measurements and, thus, of greatest potential value for tracking important, but less observable, anchor ice changes. For example, energy

budget analyses similar to those outlined in connection with Table 3, should be capable of using SWIPS water column estimates in conjunction with calibrated water-temperature and -level data to quantify local anchor ice mass production. More sophisticated analyses, directed at making frazil ice data a useful model input, are likely to require establishing relationships between anchor ice and other environmental parameters. Initial data collection for this purpose could utilize: video or single frame imagers; riverbed-based thermistor chain measurements and/or grab sampling. However, more efficient and effective data acquisition is likely to be accessible by deploying downward-looking multifrequency SWIPS instruments from the river surface in a systematic mapping mode. The acquired data would enable tracking of anchor ice thickness and internal structure (Buermans et al., 2015) simultaneously with water column profiling: to provide a quantitative basis for understanding anchor ice growth in a freezing river environment.

Acknowledgements

The authors would like to thank a helpful reviewer for constructive comments which included suggesting inclusion of water level data.

References

- Arden, R.S., Wigle, T.E., 1972. Dynamics of ice formation in the Upper Niagara River, Proc., The Role of Snow and Ice in Hydrology, IAHS-UNESCO-WMO, Banff, 1296-1313.
- Beltaos, S., 2013. *River Ice Formation*. pub. by Committee On River Ice Processes, Edmonton, AB. 552p.
- Buermans, J., Marko, J.R., Topham, D.R., Jasek, M. 2015. Ten years of SWIPS profiling in the Peace River: looking up, back, ahead and, possibly, down. Proc. 18th Workshop on the Hydraulics of Ice Covered Rivers Quebec City, QC,
- Clark, S., Doering, J., 2006. Laboratory Experiments on Frazil Size Characterizations in a Counterrotating Flume. J. Hydraulic Engineering, 94-101.
- Daly, S.F. and Axelson, K.D., 1989. Estimation of time to maximum supercooling during dynamic frazil ice formation. USA Cold Regions Research and Engineering Laboratory, Special Report 89-26.
- Dube', M., Turcotte, B., Morse, B, Stander, E., 2013. Formation and inner structure of ice dams in steep channels. Proc. 17th Workshop on River Ice, Edmonton, AB.
- Gosink, J.P., Osterkamp, T.E., 1983. Measurements and analysis of velocity profiles and frazil ice crystal rise velocities during periods of frazil-ice formation in rivers. *Annals of Glaciology* 4, 79–84.
- Hammar, L., Shen, H.T., 1995. Frazil evolution in Channels, Jour. Hydraulic Res., 33(3), 291-306.
- Hirayama, K., Terada, K., Sato, M., Hirayama, K., Saamoto, M., Yamazaki, M., 1997. Field Measurements of anchor and frazil ice, Ninth Workshop on River Ice, Fredericton, N.B., 141-151.
- Jasek, M., Marko, J.R., Fissel, D., Clarke, M., Buermans, J., Paslawski, K. , 2005. Instrument for detecting freeze-up, mid-winter and break-up processes in rivers. Proc. 13th Workshop on Hydraulic of Ice-Covered Rivers, Hanover, NH. 34 p.
- Jasek, M., Ghobrial, T., Loewen, M., Hicks, F., 2011. Comparison of CRISP1D modeled and SWIPS measured ice concentrations on the Peace River. Proc. 16th Workshop on River Ice. Winnipeg, Man.

Jasek, M., Shen, H.T., Pan, J. Paslawski, K., 2015. Anchor ice waves and their impact on winter ice cover stability. Proc. 15th Workshop on Hydraulic of Ice-Covered Rivers, Quebec City, QC. 37 p.

Kempema, E., Ettema, R., McGee, B., 2008, Insights from anchor ice formation in the Laramie River, Wyoming. Proc. 19th IAHR International Symposium on Ice, 63-76.

Kempema, E.W. and Ettema, R., 2015, Frazil or anchor ice blockages of submerged water intakes. Proc. 18th Workshop on Hydraulic of Ice-Covered Rivers, Quebec City, Canada. 14 p.

Kerr, D.J., Shen, H.T., Daly, S.F., 2002. Anchor ice growth and frazil accretion. Proc. IAHR 12th International Symposium on Ice, Trondheim, Norway, 1059-1067.

Liu, L., Li, H., Shen, H.T., Shumilak, B., 2004, Simulation of Flow and Thermal Conditions Downstream of Limestone Generating Station, Proc. 17th International Symposium on Ice, St. Petersburg, , V2, 323-331.

U. of Alberta, 2015:

<http://www.engineering.ualberta.ca/en/NewsEvents/Engineering%20News/2015/July/Coolresearchprojectsproberivericelifecycle.aspx>

Marcotte, N., Roberts, S. (1986) Elementary Mathematical Modeling of Anchor Ice, Proc., IAHR Ice Symposium, Iowa City, Iowa, 493-506.

Marko, J.R., Jasek, M., 2010a. Sonar detection and measurements of ice in a freezing river I: Methods and data characteristics. Cold Reg. Sci. Technol. 63, 121-134.

Marko, J.R., Jasek, M., 2010b. Sonar detection and measurements of ice in a freezing river II: Observations and results on frazil ice. Cold Reg. Sci. Technol. 63, 135-153.

Marko, J.R., Jasek, M., Topham, D.T., 2015a. Multifrequency Analyses of 2011-2012 Peace River SWIPS frazil backscattering data. Cold Reg. Sci. Technol. 110, 102-119.

Marko, J. R. Topham, D.R., 2015. Laboratory measurements of acoustic backscattering from polystyrene pseudo-ice particles as a basis for quantitative frazil characterization. Cold Reg. Sci. Technol. 112, 66-86.

Morse, B. and M. Richard, 2009. A field study of suspended frazil ice particles. Cold Regions Science and Technology. 55(1): 86-102.

Parkinson F.E. 1984. Anchor ice effects on water levels in Lake St. Louis, St-Lawrence River at Montreal. In: Proc. 3rd CGU-HS CRIPE Workshop on the Hydraulics of River Ice, Fredericton, NB., Canada.

Petrovich, V.V., 1956. Formation of depth-ice. Translated from Priroda 9: 94-95 by Defense Research Board, D.S.J.S., Department of National Defense, Canada, T235R.

Prowse, T.D. 1987, Monograph on River Ice Jams, River Ice Processes, NRCC Working Group on River Ice Jams.

Qu, Y.K., Doering, J. 2007. Laboratory study of anchor ice evolution around rocks and on gravel beds. Can. J. Civ. Eng. 34, 46-55.

Shen, H.T., Foltyn, E.P. and Daly S.F. 1984, Forecasting water temperature decline and freeze-up in rivers, U.S. Army, CRREL Report 84-19, Hanover, N.H.

Shen, H.T., 2005. CRISSP1D Programmer's Manual. Prepared by Department of Civil Engineering, Clarkson University, Potsdam, NY for CEA Technologies Inc.. CEATI Report No. T012700-0401.

Vogt, C., Laihem, K., Wiebusch, C., 2008. Speed of sound in bubble-free ice. J. Acoust. Soc. Am. 124, 3613-3618.

Appendix

Anchor ice production from frazil capture.

Physical capture of or deposition of suspended frazil provides the principal mechanism for anchor ice growth in the CRISSP1D model. Capture rates are assumed to be directly proportional to the local fractional volume concentration. This allows losses in suspended frazil fractional volume, F , to be expressed in terms of h the mass thickness (defined as layer thickness multiplied by $(1-P/100)$ where P = anchor ice layer porosity in per cent) as:

$$\frac{dh}{dt} = \gamma F. \quad (\text{A1})$$

The quantity h increases upwards from the riverbed while the capture coefficient, γ ,

is defined ([Jasek et al 2011](#)) as a downward velocity. Changes in the fractional volume of suspended frazil can then be written as:

$$\frac{dF}{dt} = -\frac{\gamma F}{H}, \quad (\text{A2})$$

where H is the total water depth and, for $h \ll H$, F can be approximated by h/H . A simplified model is now developed for the purpose of estimating an upper bound on the deposition coefficient γ from measured frazil distributions. The overall rate of change in suspended frazil fractional volume is expressed as:

$$\frac{dF}{dt} = \Psi(t) - \frac{\gamma F}{H}, \quad (\text{A3})$$

Where $\Psi(t)$, a measure of the energy flux driving frazil ice formation, represents the difference between the surface heat flux, Φ , and the rate of release of latent heat from ice production. If for example, only frazil ice formation provides latent heat contributions, the water column attains an equilibrium degree of super cooling which matches ice production. At the other extreme, where *in-situ* freezing is the dominant mode of ice production, the frazil ice concentration is controlled by the latent heat released by *in-situ* freezing.

The observed time variations in fractional volume, $F(t)$ described in the text, feature a rapid rise to a maximum value and a subsequent, roughly, exponential decay to a quasi-equilibrium fractional volume F_∞ . The presence of a local maximum in the solution of equation A3 requires that the function $\Psi(t)$ decrease with time.

The frazil capture coefficient γ can be obtained from the two conditions under which dF/dt vanishes: corresponding to the content peak, and the long term equilibrium state. Under these respective conditions:

$$\gamma = \frac{\Psi_p H}{F_p} \quad \text{and} \quad \gamma = \frac{\Psi_\infty H}{F_\infty}. \quad (\text{A4})$$

Neither Ψ_p or Ψ_∞ are directly accessible from experimental data, but it is possible to put an upper bound on γ by substituting Ψ_0 for Ψ_p , since, for the existence of a maximum, $\Psi(t)$ must be a decreasing function of time. This ensures that $\Psi_0 > \Psi_p$, independently of the form of the driving function and Ψ_0 can be derived from the initial rate of rise in frazil content.

The following example employs a simple exponential decay from an initial state Ψ_0 to a final equilibrium state Ψ_∞ . This function provides solutions which reproduce the characteristic form of the frazil ice profiles observed in our SWIPS studies.

For a driving function of the form $\psi(t) = \psi_0(1 + ae^{-\alpha t})$, the solution to equation A3 can be expressed in the normalized form

$$\frac{F(\tau)}{F_\infty} = (1 - e^{-\tau}) + \frac{(\Psi_0 / \Psi_\infty - 1)}{(1 - \beta)} e^{-\tau} (e^{(1-\beta)\tau} - 1), \quad (\text{A5})$$

where $\tau = H/\gamma$, and $\beta = \alpha H/\gamma$ such that β denotes the ratio of the frazil deposition time constant (H/γ), to the decay constant of the driving function (α^{-1}).

Figure A1 shows examples of solution which display features similar to those of the measured frazil events, where the concentrations are normalized by the peak value. The individual curves represent increasingly severe reductions in the driving flux ratio.

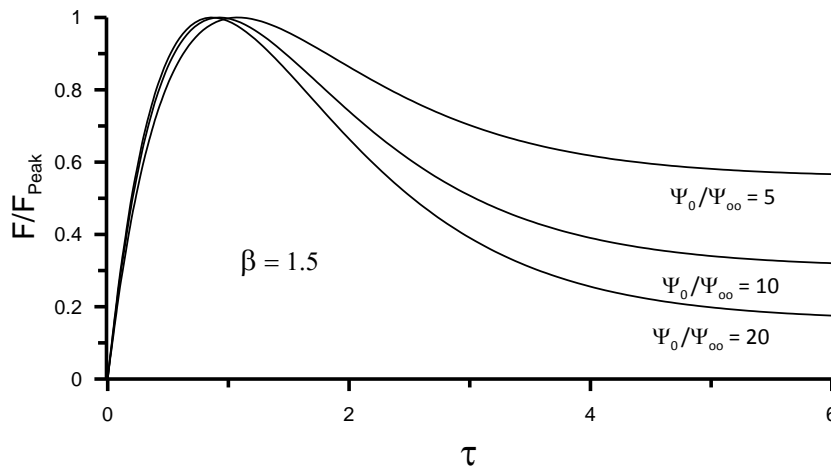


Figure A1. Frazil fractional volume solutions to equation A5 .

Table A1. The Table below lists the upper bounds of the four events examined here, calculated for $H=5$ m as described above.

Event	Ψ_0 (h^{-1})	F_{Peak}	γ (mh^{-1})	τ , (h)
Nov 20 - Nov 21	2.69E-05	4.65E-05	2.89	1.73
Jan 14 - Jan 15	3.37E-05	6.31E-05	2.67	1.87
Jan 25 - Jan 26	4.05E-05	3.05E-05	6.63	0.75
Feb 7 - Feb 8	7.75E-05	4.32E-05	8.97	0.56

The variations in the values in the Table may be an indication of the degree of over prediction associated with the upper bounds, which are influenced by the frazil ice balance. For the purpose of assessing the ability to sustain anchor ice by bottom capture, the largest value in the table, approaching 10 mh^{-1} is almost an order of magnitude larger than the largest value used in the [Jasek et al. \(2011\)](#) simulations but still is an order of magnitude below estimated anchor ice growth rates.